

DIGITAL ACCESS TO SCHOLARSHIP AT HARVARD
DASH.HARVARD.EDU

HARVARD LIBRARY


Assembly of RIG-I Signaling Complexes in Antiviral Immunity

Citation

Cadena, Cristhian. 2020. Assembly of RIG-I Signaling Complexes in Antiviral Immunity. Doctoral dissertation, Harvard University, Graduate School of Arts & Sciences.

Link

https://nrs.harvard.edu/URN-3:HUL.INSTREPOS:37365761

Terms of use

This article was downloaded from Harvard University's DASH repository, and is made available under the terms and conditions applicable to Other Posted Material (LAA), as set forth at

https://harvardwiki.atlassian.net/wiki/external/NGY5NDE4ZjgzNTc5NDQzMGIzZWZhMGFlOWI2M2EwYTg

Accessibility

https://accessibility.huit.harvard.edu/digital-accessibility-policy

Share Your Story

The Harvard community has made this article openly available.
Please share how this access benefits you. Submit a story

ASSEMBLY OF RIG-I SIGNALING COMPLEXES IN ANTIVIRAL IMMUNITY

A dissertation presented

By

Cristhian Cadena

To

The Division of Medical Sciences

In partial fulfillment of the requirements

for the degree of

Doctor of Philosophy

in the subject of

Virology

Harvard University

Cambridge, Massachusetts

April 2020

© 2020 Cristhian Cadena

All rights reserved

Dissertation Advisor: Sun Hur Cristhian Cadena

Abstract

Assembly of RIG-I Signaling Complexes in Antiviral Immunity

RIG-I is a cytosolic sensor of viral dsRNA. RIG-I molecules are recruited to and translocate along the length of the viral dsRNA, forming filaments. Filament formation initiates a signaling cascade that leads to the aggregation of the adaptor MAVS, phosphorylation and dimerization of transcription factor IRF3, and expression of IFN-β and other antiviral genes. Ubiquitination, a form of post-translational modification, is critical for the activation of RIG-I. Although structural studies give us a picture of the ubiquitinated RIG-I, the identity of the ubiquitin ligase involved in this process remains debated. Furthermore, how RIG-I is recognized as a substrate for ubiquitination remains unknown.

Our results showed that the RIPLET is the required ubiquitin ligase for RIG-I. RIPLET specifically ubiquitinated RIG-I in dsRNA-dependent manner. RIPLET bound to filamentous RIG-I in an RNA length-dependent manner and their interaction required bivalent RIPLET PRY/SPRY domains. Furthermore, RIPLET adopted an additional binding mode with long RIG-I filaments, leading to their clustering. In the absence of ubiquitination, the second binding mode of RIPLET was able to promote the aggregation of MAVS and the expression of antiviral genes in cells. These results show a previously un-recognized ubiquitin-independent role of RIPLET in antiviral signaling. Our work also highlights the importance of receptor clustering for the induction of IFN signaling.

The clustering of RIG-I filaments, as well as the prion-like polymerization of MAVS, allows the rapid amplification of signaling. Yet, the process by which the macromolecular assemblies of

RIG-I and MAVS are cleared following signaling remains poorly understood. In the last part of my work, we show that dsRNA stimulation induces the recruitment of RIG-I into atypical stress granules (SGs), which contained several IFN signaling molecules and autophagy markers. In the absence of SGs, cells are not able to degrade these signaling aggregates, leading to hyper-activation of the IFN pathway. In addition, cells lacking SGs showed pronounced caspase-dependent death in response to dsRNA stimulation. We propose that IFN signaling aggregates are degraded through autophagy, and that SGs are act as intermediates in this process. Thus, SGs play a key role preventing aberrant IFN signaling and cell death.

Table of Contents

Title Page…… i

Copyright…… ii

Abstract …… iii

Table of Contents…… v

Acknowledgements…… viii

Dedication…… x

Chapter 1: Introduction…….... 1

1.1 Self-vs-non-self-discrimination by Pattern Recognition Receptors……. 2

1.2 The RIG-I Signaling Pathway……... 3

1.3 Mechanisms of RIG-I Signaling Regulation……. 4

1.4 Filament-Like Assembly of RIG-I…….. 5

Figure 1.1: RIG-I Filament Formation and Signaling…… **7**

1.5 Ubiquitination of the RIG-I CARD…… 8

Figure 1.2: The Ubiquitination Reaction…….. 11

Chapter 2: The Role of the Ubiquitin Ligase RIPLET in the Assembly of RIG-I Signaling Aggregates in Antiviral Immune Signaling…… 12

2.1 Abstract……... 13

2.2 Introduction…… 14

2.3 Methods…… 17

2.4 Results…… 26

Figure 2.1: RIPLET, Not TRIM25, Is Required for RIG-I Signaling…… 27

Figure 2.2: RIPLET, Not TRIM25, Ubiquitinates RIG-I in a dsRNA-dependent Manner…… 31

Figure 2.3: RIPLET Recognizes Pre-Oligomerized RIG-I on dsRNA and Activates RIG-I Signaling in a dsRNA Length-Dependent Manner…… 35

Figure 2.4: RIPLET Cross-Bridges RIG-I Filaments *In Vitro*…… 39

Figure 2.5: RIPLET Cross-Bridges RIG-I Filaments in Cells Independent of Stress Granules…… 42

Figure 2.6: RIPLET-Mediated RIG-I Aggregation Enhances Antiviral Signaling, in Both Ubiquitin-Dependent and -Independent Manners…… 45

2.5 Discussion…… 46

Chapter 3: Resolution of RIG-I Signaling Aggregates in Antiviral Immunity…… 49

3.1 Abstract…… 50

3.2 Introduction…… 51

3.3 Methods…… 54

3.4 Results…… 57

Figure 3.1: RIG-I Signaling Complexes Are Recruited to SGs…… 59

Figure 3.2: SGs Suppress RIG-I Signaling…… 63

Figure 3.3: SGs Are Critical for Cell Survival After dsRNA Stimulation…… 67

3.5 Discussion…… 69

Chapter 4: Conclusion…… 71

Appendix 1: References…… 77

Appendix 2: Supplemental Figures…… 91

Supplemental Figure 1: Related to Figure 2.1…….. 92

Supplemental Figure 2: Related to Figure 2.2…….. 93

Supplemental Figure 3: Related to Figure 2.3…….. 94

Supplemental Figure 4: Related to Figure 2.4…….. 96

Supplemental Figure 5: Related to Figure 2.6…… 97

Supplemental Figure 6: Related to Figure 3.1……..98

Supplemental Figure 7: Related to Figure 3.3…… 99

Acknowledgements

I would like to first thank my mentor, Dr. Sun Hur. She helped me become a better scientist. Sun's mentorship has installed a way of thinking that I will carry throughout my scientific career. I would like to thank her for allowing me freedom to explore new ideas and topics and helping to guide me along the way. I also want to thank the past and present members of the Hur lab. I not only learned science from them, but also leaned on them for support and guidance. I want to thank them for their advice and feedback during my time in the lab.

Additionally, I would like to thank the Virology Program faculty and staff, including Dr. Sean Whelan, Dr. David Knipe, Dr. Ben Gewurz, and Maria Bollinger. Thank you to my Dissertation Advisory Committee, Dr. Jonathan Kagan, Dr. Hao Wu, and Dr. Philip Kranszuch. Their questions and suggestions during our meetings were critical to develop stronger science. I want to extend my deepest thanks to Dr. Christopher Randle at Sam Houston State University for inspiring my interest in science. I want to thank Dr. Carolina Lopez at Washington University for introducing me to the world of viruses and innate immunity. Back then, I would not have imagined that eight years later, I would be working on RIG-I. I want to express my thanks to Dr. Susan Ross of University of Illinois-Chicago, whose mentorship and ongoing support have meant so much. Dr. Ross has been an incredible mentor and I would not be where I am without her. Lastly, I would like to thank Dr. Arnaldo Diaz Vazquez of University of Pennsylvania- the opportunities provided to me by SUIP and PennPREP opened so many doors for me.

I would like to thank my classmates- their support was particularly vital during the early years of the program, and it was an honor to get to know them. I would especially like to thank future doctors Tobi (or Toby) Hermann and Tyler Krause for their friendship.

Last, but certainly not least, I want to thank my family, especially my mother. She sacrificed so much so that I could come to this country and has supported me throughout my long educational journey. I also want to thank my partner, Leah. She has been so important in every endeavor that I've taken on inside and outside of the lab. I thank her for always being there to help me- providing me with emotional support, listening to presentations, proofreading papers, and much more. Thanks for listening to me talk non-stop about RIPLET!

Dedication

I dedicate this thesis to my mother, Nancy Astudillo. You sacrificed so much to come to this country so that I could have a better education and future. I have never met a stronger person than you. I will be thankful to you for the rest of my life. Juntos lo logramos.

Chapter 1: Introduction

Higher Order Oligomerization of RIG-I-like Receptors

Portions of this chapter were published elsewhere:

Cadena C and Hur S. (2019) Filament-like assemblies of intracellular nucleic acid sensors: commonalities and differences. Molecular Cell. 76 (2), 243-254.

Author contributions:

Cadena C and Hur S conceptualized, wrote, and review this work.

1.1 Self-vs-non-self-discrimination by Pattern Recognition Receptors

The recognition of pathogens by the immune system is critical for the activation of signaling pathways that allow cells to combat infection. Cells encode receptors, known as pathogen recognition receptors (PRRs), that sense the presence of moieties or features present in pathogens (pathogen-associated molecular patterns or PAMPs) but absent in the host. The last decade of studies showed that foreign nucleic acid sensing is a central mechanism by which the innate immune system detects pathogen infection. This is carried out by several sensors that are classified as PRRs. These sensors include RIG-I-like-receptors (RLRs), some toll-like-receptors (TLRs), aim-2-like-receptors (ALRs), cGAS, among others.

The RIG-I-like receptors, which include RIG-I and MDA5, are critical for mounting the immune response against RNA virus infection. However, studies have also shown that, under various pathologic conditions, these nucleic acid sensors can misconstrue self-derived nucleic acids as foreign, and that this misrecognition underlies a growing number of auto-inflammatory diseases. At the molecular level, this makes sense considering that all nucleic acids, regardless of their origin, are made up of identical building blocks. This is unlike other immune receptors, such as TLR4, that recognize lipid moieties that are normally absent in the host. Thus, this raises the question of exactly how nucleic acid sensors in the innate immune system accurately discriminate between self vs. non-self under normal physiological conditions.

Recent findings, including our own, suggest that the assembly of higher order molecular complexes allows for accurate discrimination between self vs. non-self nucleic acids. Higher order oligomerization of receptors enables sensing of multiple distinct features in foreign

nucleic acids, including structure and length, and is critical for robust activation of immune signaling.

1.2 The RIG-I Signaling Pathway

Retinoic-acid inducible gene I (RIG-I) is a cytoplasmic sensor of viral dsRNA. RIG-I is the founding member of the RIG-I-like receptor (RLR) family, which also includes melanoma-differentiation-associated protein 5 (MDA5). RIG-I detects a broad range of viral RNAs during infection and activates an intracellular signaling pathway that leads to the production of type I interferons (Yoneyama et al., 2004). RIG-I consists of two N-terminal caspase activation and recruitment domains (CARDs), a central DExD/H-box helicase domain, and a C-terminal domain (CTD) (Fig. 1.2A). The CARDs are involved in downstream signal activation, while the helicase-CTD domains interact with dsRNA. In the resting state, the CARD signaling domain exists in an auto-repressed state, but it is released upon dsRNA and/or ATP binding (Kowalinski et al., 2011; Rawling et al., 2015). The released RIG-I CARDs interact with the CARD domain of the downstream adaptor molecule mitochondrial antiviral-signaling protein (MAVS) through a homotypic CARD-CARD interaction (Peisley et al., 2014; Wu et al., 2014). This CARD-CARD interaction then triggers MAVS filament formation, which functions as a signaling platform to recruit further downstream signaling molecules including TRAFs, TBK1 and IKK. These molecules subsequently activate IRF3/7 and NF-kB to upregulate type I interferons and other antiviral molecules (Hou et al., 2011; Jiang et al., 2012; Wu and Hur, 2015).

RIG-I senses viral dsRNA but discriminates between cellular and viral dsRNAs based on the combination of the RNA duplex structure and the 5’-triphosphate (5’ppp) moiety present in

certain viral RNAs (Hornung et al., 2006; Pichlmair et al., 2006; Schlee et al., 2009). 5'ppp is present in all nascent transcripts, whether from the host or virus, but cellular RNAs typically undergo 5'-processing in the nucleus. This often results in replacement of 5'ppp by 5'p that cannot stimulate RIG-I (Ren et al., 2019). Some viral RNAs, however, are generated in the cytoplasm and can bypass 5'-processing, thereby being subjected to RIG-I detection. The structures of monomeric RIG-I in complex with dsRNA showed that the helicase forms a C-like structure around dsRNA, while the CTD caps the dsRNA end, directly recognizing the 5'ppp moiety (Lu et al., 2010; Wang et al., 2010).

1.3 Mechanisms of RIG-I Signaling Regulation

As mentioned earlier, RIG-I remains in an auto-inhibited state in the absence of infection, wherein the CARD signaling domain is secluded within the protein. Binding of the viral dsRNA end releases the CARD signaling domain, which then interacts with the CARD domain of the adaptor MAVS. Structural studies have shown that the interaction between RIG-I and MAVS requires the homo-tetramerization of the RIG-I CARD domain (Peisley et al., 2014; Wu et al., 2014). This CARD tetramerization requirement is fulfilled through two mechanisms, RIG-I filament formation and RIG-I CARD ubiquitination. First, the assembly of filamentous oligomers allows the close proximity of multiple RIG-I molecules, thereby concentrating CARD domains and facilitating their tetramerization. Second, the K63-linked poly-ubiquitination of the RIG-I CARD promotes its tetramerization for efficient MAVS activation. I will further discuss these mechanisms below.

1.4 Filament-Like Assembly of RIG-I

In addition to 5'ppp and the duplex structure, RIG-I also recognizes dsRNA length for more accurate discrimination between self vs. non-self RNAs. Earlier studies showed that > 1kb dsRNA activates MDA5 but not RIG-I (Kato et al., 2006), which led to a model that MDA5 recognizes long dsRNA while RIG-I recognizes short dsRNA. However, a number of studies showed that RIG-I recognizes longer dsRNAs when compared among <~1 kb and provided at the same molar concentration, i.e. with the same concentration of 5'ppp (Binder et al., 2011; Patel et al., 2013). Direct association studies have not yet shown which physiologically relevant ligands are sensed by RIG-I during infection. Therefore, the duplex length discrimination hypothesis is based on studies using model dsRNA ligands. However, this duplex length-dependence can explain how different strains of Sendai virus (SeV) that generate defective viral genomes (DVGs) of different lengths activate RIG-I in a length-dependent manner (Strahle et al., 2006).

How does RIG-I senses dsRNA length? The answer likely lies in the fact that dsRNA binding is not sufficient to activate RIG-I and that RIG-I CARD oligomerization is additionally required for MAVS activation. The helicase domain of RIG-I contains an active site for ATP binding and hydrolysis, which is important for RIG-I translocation and oligomerization on dsRNA (Myong et al., 2009; Patel et al., 2013; Peisley et al., 2013). While RIG-I binds to 10-15 bp dsRNA end as a monomer (Jiang et al., 2011; Kowalinski et al., 2011; Luo et al., 2011), RIG-I forms a filamentous oligomer on longer dsRNA (Binder et al., 2011; Patel et al., 2013; Peisley et al., 2013). More specifically, RIG-I preferentially binds to the dsRNA end as a monomer, but this triggers RIG-I ATP hydrolysis, which powers RIG-I translocation from the dsRNA end to the

interior (Myong et al., 2009). RIG-I translocation then re-exposes the 5'ppp, allowing recruitment of another RIG-I molecule to the dsRNA end. Subsequently, iterations of end-recruitment and translocation of RIG-I leads to formation of filamentous oligomerization near the dsRNA end (Fig. 1.2B) (Peisley et al., 2013). Filament assembly of RIG-I then brings together CARDs from adjacent RIG-I molecules in close proximity, and consequently promotes CARD tetramerization (Fig. 1.2B) (Peisley et al., 2013). RIG-I filament formation is limited on >1 kb dsRNAs, because the assembly initiates from the dsRNA end to the interior, and the dsRNA ends become a limiting factor with very long dsRNA (Peisley et al., 2013). This explains why RIG-I signaling is inefficient with >1 kb dsRNA. RIG-I filament assembly may also provide an explanation as to how RIG-I senses RNA modifications present in the RNA interior distant from the dsRNA end (Hornung et al., 2006; Peisley et al., 2013; Uzri and Gehrke, 2009).

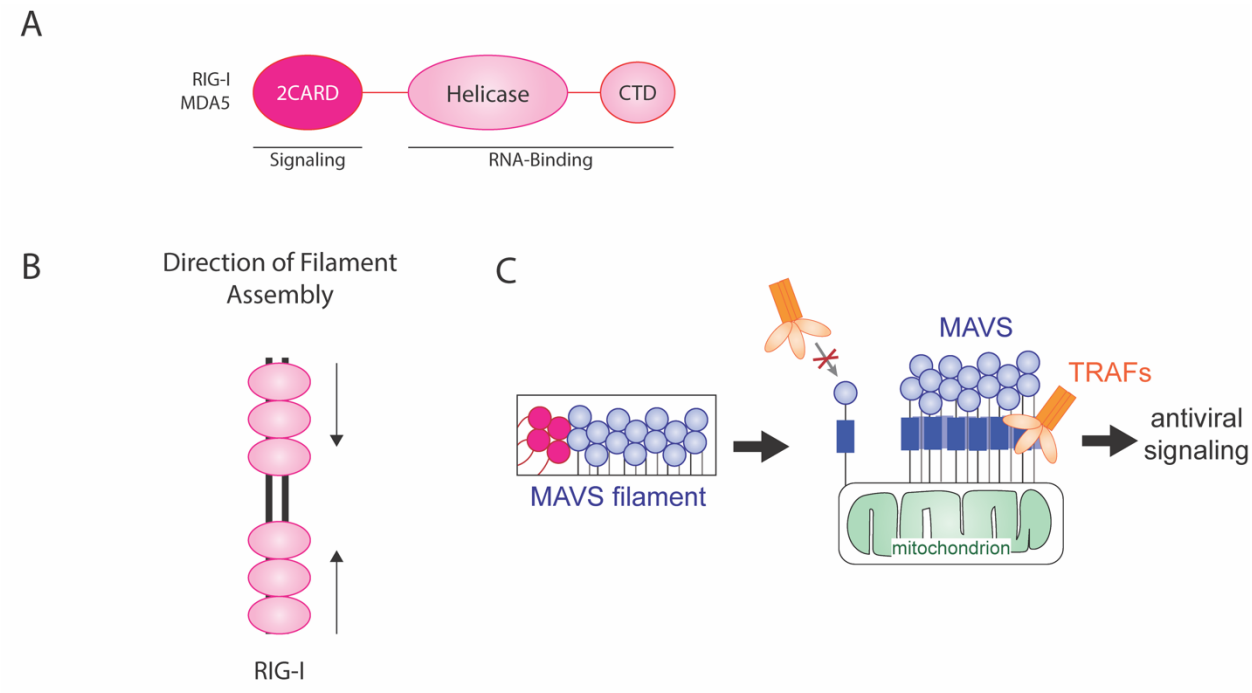


Figure 1.1: RIG-I Filament Formation and Signaling

1.1A) Both RIG-I and MDA5 share the same domain architecture, comprising a 2CARD signaling domain, a Rec-A-like helicase, and a C-terminal domain. **1.1B)** RIG-I first binds the 5'ppp at the end of the dsRNA, then uses ATP hydrolysis to translocate to the interior. Repeated 5'ppp end binding and translocation leads to 'coating' of the dsRNA and filament formation along its length. **1.1C)** RIG-I filament formation promotes signaling by concentrating available 2CARD domains for tetramerization. The 2CARD tetramer promotes MAVS filament formation, which in turns recruits downstream signaling molecules like TRAFs.

1.5 Ubiquitination of the RIG-I CARD

Ubiquitination is a type of post-translational modification that is involved in many cellular processes, including protein degradation, trafficking, protein-protein interactions, and signal transduction, among many others. During this process, the small protein ubiquitin (~8.5kd) is covalently conjugated to a target through the sequential activity of three enzymes, E1, E2, and E3 (figure 1.2). The first step in this cascade involves the ubiquitin activating enzyme (E1), which uses ATP to conjugate the C-terminal glycine residue in ubiquitin to its active cystine. Next, ubiquitin is transferred to a cystine residue in the active site of an ubiquitin-conjugating enzyme (E2). Finally, the ubiquitin ligase (E3) binds to both, the E2 and the substrate, and facilitates the transfer of ubiquitin from the E2 to a lysine residue in the target protein (Komander D and Rape M, 2012). Since E3s are responsible for binding the substrate, they are critical determinants of the specificity of ubiquitination.

The ubiquitin protein contains seven lysine residues (6, 11, 27, 29, 33, 48 and 63) that can be targeted for ubiquitination. Repeated ubiquitination of the same target molecule leads to either mono-ubiquitination at different sites, or the formation of poly-ubiquitin chains. The lysine residue targeted within the ubiquitin protein during poly-Ub chain formation also plays a role in the fate of the target protein. Repeated ubiquitination at lysine 48, for example, is a typical mark for proteasomal degradation of the target protein, while ubiquitination at lysine 63 is associated with signal transduction. K63-linked poly-ubiquitination plays a role in multiple immune signaling pathways, including the activation of RIG-I during viral infection.

Structural studies have provided a clear picture of the role of ubiquitination in RIG-I signaling, specifically in CARD tetramerization. RIG-I filament formation on long dsRNAs (>100bp) concentrates the number of RIG-I molecules available for CARD tetramerization and signaling. However, RIG-I can also signal with shorter dsRNAs (between 15-50bp). The structure of the RIG-I CARD tetramer bound to K63-linked poly-Ub chains revealed how stable CARD tetramerization on shorter dsRNAs is achieved. The RIG-I CARD tetramer structure exhibited a helical assembly resembling a 'lock washer' (Peisley et al., 2014). This helical assembly is bound at the periphery by K63-linked poly-Ub chains, which stabilize the CARD tetramer (Figure 1.2, adapted from Peisley et al., 2014). The RIG-I CARD tetramer serves as a template to recruit MAVS CARDs and nucleate the assembly filaments, which in turn initiate antiviral signaling (Wu et al., 2014). Despite the detailed understanding of the ubiquitinated RIG-I CARD, we are missing critical insight into the ubiquitination process, specifically, which E3 ubiquitinates RIG-I during signaling and how this E3 recognizes RIG-I as a substrate (figure 1.2).

The ubiquitination of RIG-I was demonstrated shortly after its discovery. The ubiquitin ligase TRIM25 was shown to ubiquitinate RIG-I at lysine 172 in the CARD domain (Gack et al., 2007). TRIM25 was discovered using a pull-down mass-spectrometry approach using the isolated RIG-I CARD fused to GST (GST-CARD), which is sufficient to initiate RIG-I signaling. Deletion of TRIM25 in cells led to higher viral replication and a deficiency in the expression of antiviral genes, demonstrating a critical role for this E3 in antiviral signaling (Gack et al., 2007). RIPLET (also known as REUL) is a second ubiquitin ligase shown to interact with RIG-I (Gao et al., 2009; Oshiumi et al., 2009). This interaction was demonstrated using a yeast-two-hybrid approach with full-length RIG-I as a bait. Surprisingly, RIPLET was shown to ubiquitinate RIG-I at

the same lysine residue in one study (Gao et al., 2009), but also at several other C-terminal lysine residues (Oshiumi et al., 2009; Oshiumi et al., 2010, Oshiumi et al., 2013). Like TRIM25, deletion of RIPLET from cells led to a deficiency in antiviral signaling. The redundancy in the function of these ubiquitin ligases led to a model in which RIPLET and TRIM25 sequentially ubiquitinate RIG-I during antiviral signaling. In this model, RIPLET first ubiquitinates C-terminal residues of RIG-I, which was thought to relieve the auto-repression of the N-terminal CARD domain. Second, RIG-I dsRNA binding allows the recruitment of TRIM25, which then ubiquitinates the CARD domain at lysine 172, promoting signaling (Oshiumi et al., 2010).

The sequential ubiquitination model fails to take into account that dsRNA binding alone is sufficient to release the RIG-I CARD (Kowalinski et al., 201), without the need for ubiquitination. Furthermore, the role of TRIM25 in RIG-I signaling has been studied mostly in the context of GST-CARD overexpression, thus whether or not TRIM25 plays a role in the signaling of full-length endogenous RIG-I remained unknown. In addition, the antiviral role of TRIM25 in the context of IAV infection (a RIG-I-specific agonist) was shown to be RIG-I-independent (Meyerson et al., 2017), and TRIM25 has ascribed with several other antiviral functions (Choudhury et al., 2014; Li et al., 2017; Manokaran et al., 2015; Zheng et al., 2017). Altogether, these findings suggest that the effect of TRIM25 on RIG-I signaling could be indirect. The conflicting reports about the role of RIPLET and TRIM25 in RIG-I signaling prompted us to study the mechanistic details of RIG-I ubiquitination.

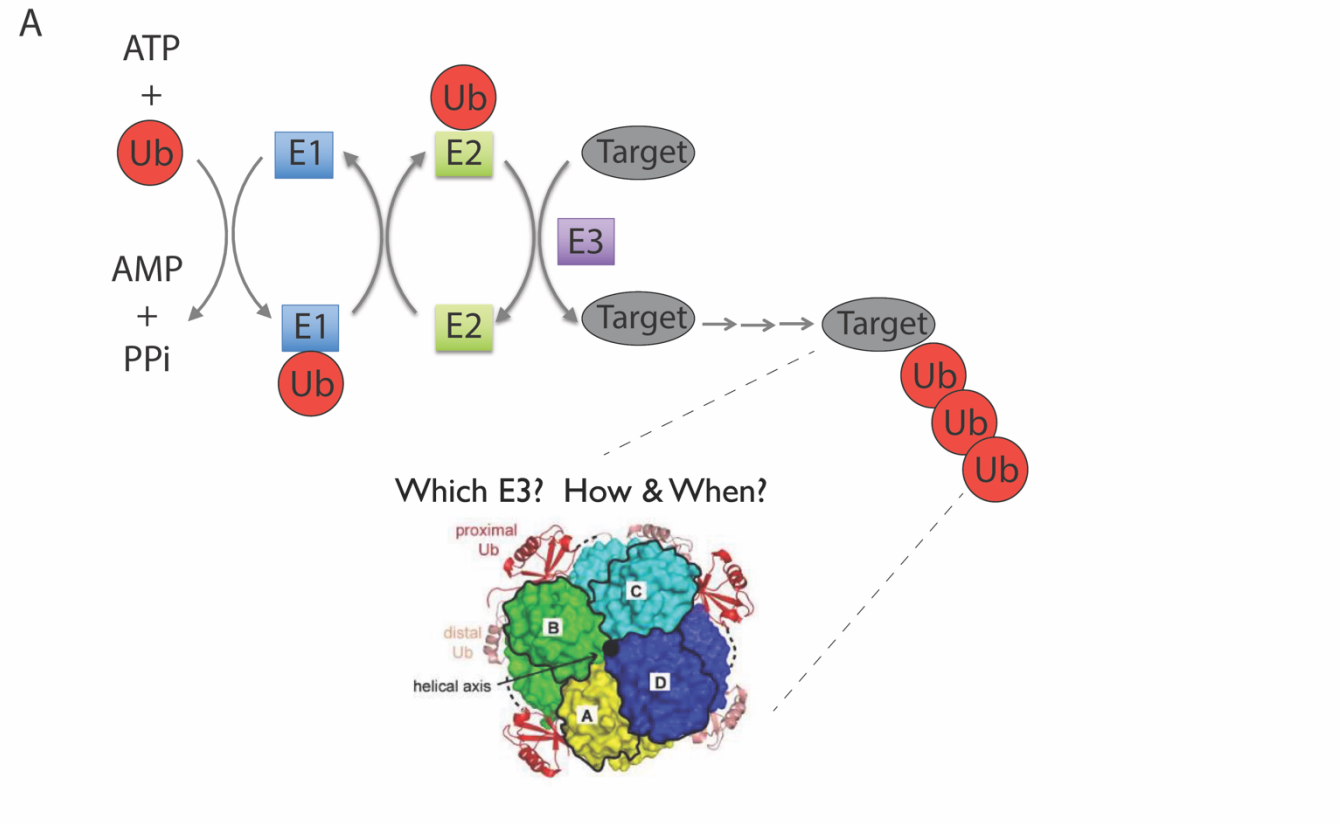


Figure 1.2: The Ubiquitination Reaction

1.2A) The ubiquitin activating enzyme uses ATP to activate ubiquitin to conjugate the C-terminal glycine residue into its active site. Ubiquitin is then transferred to the ubiquitin-conjugating enzyme (E2). The ubiquitin ligase (E3) brings the substrate and E2 together, facilitating the final transfer of ubiquitin to the target. Below is the structure of the RIG-I CARD tetramer (A-D) bound by a K63-linked poly-ub chain at the periphery (adapted from Peisley et al., 2014). Despite having a detail picture of the ubiquitinated target in RIG-I signaling (CARD), we are missing key information in the ubiquitination reaction.

Chapter 2:

The role of the ubiquitin ligase RIPLET in the assembly of RIG-I signaling aggregates in antiviral immune signaling.

A version of this chapter was published elsewhere:

Cadena C, Ahmad S, Xavier A, Willemsen J, Park JW, Oh SW, Fujita T, Hou F, Binder M, and Hur S. Ubiquitin-dependent and -independent roles of E3 ligase RIPLET in innate immunity. *Cell*. 177(5), 1187-1200 (2019)

Author Contributions:

CC, SA, AX, JW, JWP, MB and SH designed experiments and analyzed data. CC, SA, AX, JW, SP and JWP performed experiments. SWO and TF provided RIG-I antibody. FH and MB provided knock-out cell lines and FH provided RIPLET antibody.

2.1 Abstract

The conventional view posits that E3 ligases function primarily through conjugating ubiquitin (Ub) to their substrate molecules. We report here that RIPLET, an essential E3 ligase in antiviral immunity, promotes the antiviral signaling activity of the viral RNA receptor RIG-I through both Ub-dependent and -independent manners. RIPLET uses its dimeric structure and a bivalent binding mode to preferentially recognize and ubiquitinate RIG-I pre-oligomerized on dsRNA. In addition, RIPLET can cross-bridge RIG-I filaments on longer dsRNAs, inducing aggregate-like RIG-I assemblies. The consequent receptor clustering synergizes with the Ub-dependent mechanism to amplify RIG-I-mediated antiviral signaling in an RNA-length dependent manner. These observations show the unexpected role of an E3 ligase as a co-receptor that directly participates in receptor oligomerization and ligand discrimination. It also highlights a previously unrecognized mechanism by which the innate immune system measures foreign nucleic acid length, a common criterion for self vs. non-self nucleic acid discrimination.

2.2 Introduction

Effective immune response to viral infection depends on the efficient recognition of viral RNAs by an innate immune receptor, RIG-I. RIG-I detects a broad range of viral RNAs, by recognizing double-stranded RNA (dsRNA) harboring a 5'-triphosphate (5'ppp) or diphosphate group (Goubau et al., 2014; Schlee et al., 2009). These features are often present in viral RNAs, either in the form of defective interfering particles or in viral genomes, but are typically absent in cellular RNAs. Viral RNA recognition then leads to the activation of the downstream adaptor molecule, MAVS, which triggers antiviral signaling pathways to produce type I and III interferons (IFNs) and other inflammatory cytokines (Yoneyama and Fujita, 2010).

Previous structural and biochemical studies have revealed a detailed picture of how RIG-I recognizes dsRNA with 5'ppp and how viral RNA binding leads to signal activation (Lassig and Hopfner, 2017; Rawling and Pyle, 2014; Sohn and Hur, 2016). In the absence of viral RNA, RIG-I is in an auto-repressed state wherein the signaling domain, the N-terminal tandem CARD (2CARD), is inhibited from activating MAVS (Kowalinski et al., 2011). dsRNA binding occurs via the RIG-I helicase domain and the C-terminal domain (CTD), which together bind the dsRNA end and recognize the 5'ppp (Jiang et al., 2011; Luo et al., 2012). dsRNA binding and/or the subsequent ATP binding was proposed to release the auto-repression of 2CARD (Kowalinski et al., 2011; Rawling et al., 2015). The released 2CARD then forms a tetramer and recruits MAVS through a homotypic CARD-CARD interaction (Jiang et al., 2012; Peisley et al., 2014). This interaction nucleates MAVS CARD filament formation, which in turn serves as a signaling platform to recruit and activate downstream signaling molecules, such as TBK1 and IRF3 (Hou et al., 2011; Wu et al., 2014).

The notion that RIG-I signaling requires not only a release of 2CARD but also its tetramerization is supported by the presence of multiple mechanisms that tightly regulate the 2CARD tetramerization process. First, while RIG-I binds to dsRNA ends as a monomer, it can also form filamentous oligomers on longer dsRNA through ATP-driven translocation of individual monomers from the dsRNA end to the interior (Binder et al., 2011; Devarkar et al., 2018; Myong et al., 2009; Patel et al., 2013; Peisley et al., 2013). It was further shown that filament formation of RIG-I promotes 2CARD tetramerization, presumably by increasing the local concentration of 2CARD (Peisley et al., 2013). Second, in addition to RIG-I filament formation, K63-linked polyubiquitin (K63-Ubn) was also shown to promote RIG-I signaling (Jiang et al., 2012). Structural studies further showed that K63-Ubn chains bind the periphery of the core 2CARD tetramer, bridging the adjacent subunits and stabilizing its assembly (Peisley et al., 2014). The 2CARD tetramer then acts as a helical template to nucleate the MAVS filament formation for downstream signal activation (Wu and Hur, 2015).

Despite the detailed understanding of the action of K63-Ubn on RIG-I, much remains debated as to how and when Ub is placed on RIG-I, which E3 ligase is involved and how it interplays with RIG-I filament formation. Previous studies reported that TRIM25 and RIPLET (i.e. RNF135) are two essential E3 ligases important for RIG-I signaling (Gack et al., 2007; Gao et al., 2009; Oshiumi et al., 2009; Oshiumi et al., 2010). A more recent study proposed that RIPLET and TRIM25 sequentially act on RIG-I upon viral RNA engagement (Oshiumi et al., 2013). That is, RIPLET first acts on the C-terminal portion of RIG-I, releasing 2CARD, which is then modified by TRIM25. However, given the previous finding that RNA binding is sufficient to release 2CARD (Kowalinski et al., 2011), it was unclear whether RIPLET indeed acts to release 2CARD and if so,

how. At the same time, accumulating evidence suggested that TRIM25 has multiple, RIG-I-independent antiviral functions (Choudhury et al., 2014; Li et al., 2017; Manokaran et al., 2015; Meyerson et al., 2017; Zheng et al., 2017), raising the question whether the observed effect of TRIM25 on RIG-I represents a direct or an indirect effect.

We here report a combination of cellular and biochemical data showing that RIG-I activation is dependent on RIPLET, not TRIM25, and that RIPLET suffices to ubiquitinate and activate RIG-I. In addition, RIPLET recognizes the filamentous form of RIG-I using two distinct binding modes, the interplays of which offer previously unrecognized mechanisms for ligand discrimination and receptor clustering.

2.3 Methods

2.3.1 Cell lines

Unless mentioned otherwise WT, RIG-I-/-, RIPLET-/- and TRIM25-/- 293T and MEF cell lines generated by the CRISPR/Cas9 technology from the Hou lab (Shi et al., 2017) were used throughout the manuscript. Additional RIPLET-/- and parental WT MEF cell lines in Figure S1 were obtained from the Oshiumi lab (Oshiumi et al., 2010). Also used in this study (Figure S1) are TRIM25-/- and parental WT MEFs from the Gack lab (Gack et al., 2007). RIPLET-/- MEFs stably expressing mouse RIPLET or ΔRING were also obtained by lentivirus transduction and selection with 1 μg/ml neomycin (see Viruses). In all cases, parental, passage-matched cell lines were compared for the effect of knock-out or complementation.

2.3.2 Plasmids

Mammalian and bacterial expression plasmids for RIG-I, MDA5 and MAVS and their truncation variants were described previously (Peisley et al., 2013; Wu et al., 2013). Human RIPLET, ΔRING (residues 94-433), ΔPSpry (residues 1-237) and PSpry (residues 249-433) were inserted between BamHI and EcoRI of pcDNA3-HA. GST-PSpry was generated first by inserting PSpry (residues 249-443) into pGEX6p-1 between BamHI and SalI. GST-PSpry in pGEX6p-1 was then amplified and inserted into pcDNA3-HA using the EcoRI site (for both 5' and 3' end restrictions). ΔRING was mutated into V127L (GTA→CTC) and T189E/S190F (ACTTCC→GAATTC) to engineer XhoI and EcoRI sites, respectively, and the sites were used to replace RIPLET CC by MCC and GCC (Figure S4D). Note that V127L (GTA→CTC) and T189E/S190F (ACTTCC→GAATTC) alone did not impact the function of RIPLET. Bacterial expression constructs for RIPLET, ΔRING

and GCC-PSpry were generated using BamHI and SalI in pET47b. RIPLET ΔPRYSPRY (residues 1-237) was inserted in pET47b using BamHI and EcoRI sites. MCC-PSpry was cloned using BamHI and SalI in pET50b. GST-PSpry was expressed from pGEX6p-1. Human TRIM25 was cloned between EcoRI and XbaI in pcDNA3-HA vector (pcDNA3 with the HA-tag between KpnI and BamHI). Baculovirus expression construct for human TRIM25 was a generous gift from Owen Pornillos's lab. The bacterial expression construct for mouse E1 ubiquitin activating enzyme (pET28-mE1) was purchased from Addgene. Human Ubc13 and Uev1A were inserted between the XmaI and XhoI restriction sites in pET47b, and human ubiquitin (WT, K63R, K48R) were inserted between the XmaI and HindIII restriction sites in pET47b. Human ubiquitin (K63only) was purchased from AddGene and subcloned into pcDNA3 with the N-terminal His-tag.

2.3.3 Viruses

Viruses SeV (Cantell strain) was purchased from Charles River. VSV (Indiana stain) was a generous gift from Dr. Sean Whelan (Harvard). EMCV (murine) was purchased from ATCC (VR-129B). To generate RIPLET-/- MEFs stable cell lines, HA-tagged mouse RIPLET or ΔRING were cloned into pBABE-Neo (kindly provided by Jim DeCaprio) using the restriction sites BamHI and EcoRI. 293T cells were transfected with the following three plasmids: pBABE-Neo, MLV Gag (gift from Dr. James DeCaprio), and pMD2.G VSV-G in a 10:10:1 ratio. Lentiviruses were harvested 48hrs post transfection. RIPLET-/- MEFs (from Oshiumi's lab) were infected with the 0.45 μM filtered supernatants for 48 hrs, then selected with 1 μg/ml neomycin. Single clones were selected by limiting dilution and confirmed by western blot.

2.3.4 Recombinant Proteins

Human RIG-I and MDA5 variants were expressed and purified as previously reported (Ahmad et al., 2018; Peisley et al., 2013). Briefly, the proteins were expressed in BL21(DE3) at 20˚C for 16-20 hr following induction with 0.5 mM IPTG. Cells were lysed by high pressure homogenization using an Emulsiflex C3 (Avestin), and the protein was purified by a combination of Ni-NTA and heparin affinity chromatography and size exclusion chromatography (SEC) in 20 mM Hepes, pH 7.5, 150 mM NaCl and 2 mM DTT. Human RIPLET and its variants were also expressed and purified in the same manner and purified by a combination of Ni-NTA and SEC. Human TRIM25 was expressed from SF9 insect cells and purified as previously described (Sanchez et al., 2016). Mouse E1, human Ubc13 and Uev1A and ubiquitins were prepared as previously reported (Peisley et al., 2013).

For N-terminal fluorescent labeling of RIG-I and its variants, the protein (~2 mg/ml) was incubated with 0.5 mM peptide (LPETGG) conjugated with fluorescein (Anaspec) and 1.5 μM S. aureus sortase A (a gift from Hidde Ploegh, MIT) (Antos et al., 2009) at 4˚C for 4 hrs, followed by reverse Ni-NTA affinity purification and/or SEC to remove sortase.

2.3.5 Synthesized RNAs

Double-stranded RNAs (dsRNAs) were prepared by in vitro T7 transcription as previously described (Peisley et al., 2011). Unless mentioned otherwise, all dsRNAs contain 5’ppp and blunt end. The sequences of 28, 42, 62, 112, 162 and 512 bp dsRNAs were taken from the first 16, 30, 50, 100, 150 and 500 bp of the MDA5 gene flanked by 5’-gggaga and 5’-tctccc. The sequences of 15 bp and 21 bp dsRNAs are 5’-agggcccgggaugcu and 5’-gagucacgacguuguaaaaaa,

respectively. The two complementary strands were co-transcribed, and the duplex was separated from unannealed ssRNAs by 15% acrylamide (15 and 21 bp), 8.5% acrylamide (28-162 bp) or 6% acrylamide (512 bp) gel electrophoresis in TBE buffer. RNA was gel-extracted using the Elutrap electroelution kit (Whatman), ethanol precipitated, and stored in 20 mM Hepes, pH 7.0. Qualities of RNAs were analyzed by 1X TBE polyacrylamide gel.

For 3'-biotin labeling of RNA, the 3' end of RNA was oxidized with 0.1 M sodium periodate in 0.25 M NaOAc, pH 5.5, at room temperature for 2 h. The reaction subsequently was treated with 0.2 M KCl, the buffer was replaced with 0.25 M NaOAc, pH 5.5, using Zeba desalting column (Pierce), and incubation EZ-Link Hydrazide-PEG4-Biotin (Pierce) continued at room temperature for 4–6 h. The labeled RNA was desalted twice to remove unincorporated biotin and was stored in 20 mM Hepes, pH 7.0, at -20 °C.

2.3.6 Antibodies

For immuno-blotting, antibodies and their manufacturers were: Rabbit α-RIG-I (ENZO), rabbit α-HA (Cell Signaling), rabbit α-β-actin (Cells Signaling) mouse α-TRIM25 (BD), mouse α-Ub (Santa Cruz), α-RIPLET (in-house). For immunofluorescence, antibodies included: α-RIG-I (in-house)(Oh et al., 2016) and α-TIAR (Santa Cruz).

2.3.7 Luciferase reporter assay

For the IFNβ promoter reporter assay, HEK293T cells were maintained in 48-well plates in Dulbecco's modified Eagle medium (Cellgro) supplemented with 10% fetal calf serum and 1% penicillin/streptomycin. At ~80% confluence, cells were transfected with plasmids encoding the IFNβ promoter driven firefly luciferase reporter plasmid (100 ng) and a constitutively expressed

Renilla luciferase reporter plasmid (pRL-CMV, 10 ng) by using lipofectamine 2000 (Life) according to the manufacturer's protocol. Unless mentioned otherwise, signaling activity of endogenous RIG-I was measured. In Figure 2.1D, expression plasmid for RIG-I (10 ng), MDA5 (5 ng), MAVS (25 ng) or GST-2CARD (50 ng), was transfected together with the reporter plasmids. In the experiments requiring RNA stimulation, the medium was changed 6hr after the first transfection and the cells were additionally transfected with RNA (0.2 μg, Invivogen). Cells were lysed ~20 hrs post-stimulation and IFNβ promoter activity was measured using the Dual Luciferase Reporter assay (Promega) and a Synergy2 plate reader (BioTek). Firefly luciferase activity was normalized against Renilla luciferase activity.

2.3.8 RT-qPCR

Unless mentioned otherwise, endogenous RIG-I signaling activity was measured by measuring the level of mRNAs for IFN-β or indicated IFN-stimulated genes. HEK293T cells were stimulated with dsRNA in a similar manner in the luciferase assay. For SeV infection, cells were treated with SeV (100 HA units/ml, Charles River) with 1 hr of absorption. For EMCV infection, MEFs were treated with the virus at a MOI = 0.1 with 1 hour absorption. Cells were lysed ~20 hr post-infection. Total RNAs were extracted using TRIzol reagent (Thermo Fisher) and cDNA was synthesized using High Capacity cDNA reverse transcription kit (Applied Biosystems) according to the manufacture's instruction. Real-time PCR was performed using a set of gene specific primers (see the Table S1), a SYBR Green Master Mix (Applied Biosystems), and the StepOne™ Real-Time PCR Systems (Applied Biosystems).

2.3.9 Ubiquitination reaction

RIG-I ubiquitination was performed in the following manner. Purified RIG-I (1.0 μM) was first incubated with dsRNA (2 ng/μl) in buffer A (20 mM Hepes, pH 7.5, 150 mM NaCl, 1.5 mM MgCl2, 2 mM ATP and 2 mM DTT) at RT for 15 min. The RIG-I:RNA complex (to the final RIG-I concentration of 0.5 μM) was then further incubated with 20 μM ubiquitin, 1 μM mE1, 5 μM Ubc13, 2.5 μM Uev1A and 0.25 μM E3 (RIPLET or TRIM25) in buffer B (20 mM HEPES pH 7.5, 1.5 mM MgCl2, 5 mM ATP and 0.6 mM DTT) at 37˚C for 30 min. For isoT treatment, isoT (10 ng/μl final) was added to the ubiquitination reaction, and further incubated at 37˚C for 30 min. Reactions were quenched with SDS loading buffer, boiled at 96 C for 5 min, and analyzed on SDS-PAGE by anti-RIG-I or anti-Ub western blot.

2.3.10 Electron Microscopy

RIG-I or RIG-IΔN (0.5 μM) was incubated with RNA (1 ng/μl) in buffer A at RT for 15 min followed by addition of RIPLET, ΔRING or its CC-swap variants (0.5 μM) and further incubated at RT for 15 min prior to EM grid preparation. Prepared samples were adsorbed to carbon-coated grids (Ted Pella) and stained with 0.75% uranyl formate as described (Ohi et al., 2004). Images were collected using a Tecnai G2 Spirit BioTWIN transmission electron microscope at 30,000x magnification for RIG-I filaments and 4,800x or 6,800x for MAVS filaments. Grids for the MAVS filaments were prepared and imaged as with the RIG-I filaments.

2.3.11 Native gel shift assays

For RNA binding assays, dsRNA (1 ng/μl) was incubated with protein (at indicated concentration) in buffer A at RT for 10 min, and the complex was analyzed on Bis-Tris native

PAGE (Life Technologies) after staining with SybrGold stain (Life Technologies). For RIG-I binding assays, fluorescein-labeled RIG-I was first incubated with dsRNA (1 ng/μl) and subsequently with RIPLET (at indicated concentration) prior to analysis by Bis-Tris native PAGE (Life Technologies). SybrGold or fluorescein fluorescence was recorded using the scanner FLA9000 (Fuji) and analyzed with Multigauge (GE Healthcare).

2.3.12 Streptavidin pull-down assay

RIG-IΔN filaments (0.5 μM) were formed on non-biotinylated 162 bp dsRNA (1 ng/μl) and 3'-biotinylated 112 bp dsRNA (1 ng/μl), and were incubated with an increasing concentrations of ΔRING or GST-PSpry (0.25, 0.5, and 1μM) at RT for 15 min in buffer A. The reaction (250 μl) was further incubated with streptavidin-agarose (15 μl, NEB), washed three times with 0.5 ml buffer A, and eluted with 1 unit/ml protease K (NEB). Biotinylated 112 bp dsRNA was purified using streptavidin beads and co-purification of 162 bp dsRNA was analyzed on the 6% TBE gel. Gel image was taken using SybrGold stain fluorescence.

For cellular streptavidin pull-down experiments, WT and RIPLET-/- 239T cells were treated with 100 ng/mL cyclohexamine for 1 hr, and then transfected with non-biotinylated 162 bp dsRNA (1 μg) and 3' biotinylated 112 bp dsRNA (1 μg). Cells were harvested 4 hrs post-transfection in the hypotonic lysis buffer (20 mM Tris, pH 7.5, 10 mM KCl, 1.5 mM MgCl2, 250 mM sucrose) and lysed using a 25G syringe (5X). Supernatants were cleared first at 500g for 4 minutes, then at 10000g for 4 minutes. The cleared lysate (400 μl) was incubated with 50 μl streptavidin-magnetic beads (NEB) overnight. The beads were washed with 500 μl of hypotonic lysis buffer (2X), 500 μl of wash buffer (0.5M NaCl, 20mM Tris-HCl, pH 7.5, 1mM EDTA), and 200 μl of ice-

cold low salt buffer (0.15M NaCl, 20mM Tris-HCl, pH 7.5, 1mM EDTA). RNA was eluted in 30 μl of elution buffer (10mM Tris-HCl pH 7.5, 1mM EDTA) at 65˚C for 5 min, then purified using TRIzol reagent. cDNA was synthesized using High Capacity cDNA reverse transcription kit with 162bp dsRNA-specific primers, and qPCR was performed as described above.

2.3.13 Immunofluorescence imaging

293T cells were infected with SeV or stimulated with 162 bp dsRNA with 5'ppp. At indicated time points post RNA stimulation, cells were fixed with 2% paraformaldehyde at RT for 10 minutes, and permeabilized with 0.5% Triton-X at RT for 10 minutes. Cells were blocked for 30 min at RT with 1% BSA in PBST, and stained using RIG-I (1:100, in-house antibody) and TIAR (1:100, SC-398372) overnight. Images were obtained using a Zeiss Axio Imager M1 microscope at 100X magnification.

2.3.14 Multi-Angle Light Scattering (MALS)

The molecular masses of RIPLET, ΔRING and PSpry were determined by MALS using a Superose 200 10/300 column (GE) attached to a miniDAWN TRI-STAR detector (Wyatt Technology) in 20 mM Hepes, pH 7.5, 150 mM NaCl, 2 mM DTT and the data was analyzed using Astra V (Wyatt Technology).

2.3.15 Quantification and Statistical analysis

Average values and standard deviations were calculated using Microsoft excel and SPSS (IBM). The values for n represent biological replicates for cellular experiments or individual samples for biochemical assays. For immunofluorescence experiments, n represent the number

of cells counted. About 300 cells were examined for each time point per sample. For each figure, the number of replicates is indicated in the figure legends. Unless otherwise mentioned, cell culture assays were performed in 3 independent experiments. p values were calculated using the two-tailed unpaired Student's t test. We consider values * $p < 0.05$, ** $p < 0.01$, ***$p < 0.001$ significant.

2.4 Results

2.4.1 RIPLET is Required for RIG-I signaling.

To examine the importance of RIPLET and TRIM25 in RIG-I functions, we first measured the signaling activity of RIG-I in wild-type (WT) 293T cells and those lacking RIG-I, RIPLET or TRIM25 (Shi et al., 2017). Cells were stimulated with either in vitro transcribed 42 bp dsRNA with 5'ppp (Figure 2.1A) or Sendai virus (SeV) (Figure 2.1B), stimuli known to trigger RIG-I signaling. Comparison of the level of mRNAs for IFN-β or IFN-stimulated genes (ISGs) showed that RIG-I and RIPLET are required for antiviral signaling in response to 5'ppp-dsRNA and SeV. TRIM25, however, was not required as TRIM25-/- cells displayed slightly enhanced antiviral signaling. Similar activities were observed with the IFN-β promoter driven luciferase activity assay (Figure 2.1C). RIPLET-/- 293T cells were normal in MDA5- and MAVS-mediated signaling (Figure 2.1D), suggesting that the defect in antiviral signaling is specific to RIG-I. Impaired RIG-I signaling in RIPLET-/- 293T was restored by complementation with RIPLET (Figure 2.1E), further supporting the notion that RIPLET, not TRIM25, is required for RIG-I signaling.

The importance of RIPLET and the non-essential role of TRIM25 in RIG-I signaling was also observed with mouse embryonic fibroblasts (MEFs). Stimulation of MEFs with 5'ppp-dsRNA or vesicular stomatitis virus (VSV) triggered antiviral signaling as measured by the induction of IFN-β mRNA (Figure 2.1F). This antiviral signaling activity depended on RIG-I and RIPLET, but not TRIM25, in agreement with the previous report (Shi et al., 2017). Complementation with RIPLET restored the antiviral signaling activity in RIPLET-/- MEFs (Figure 2.1G).

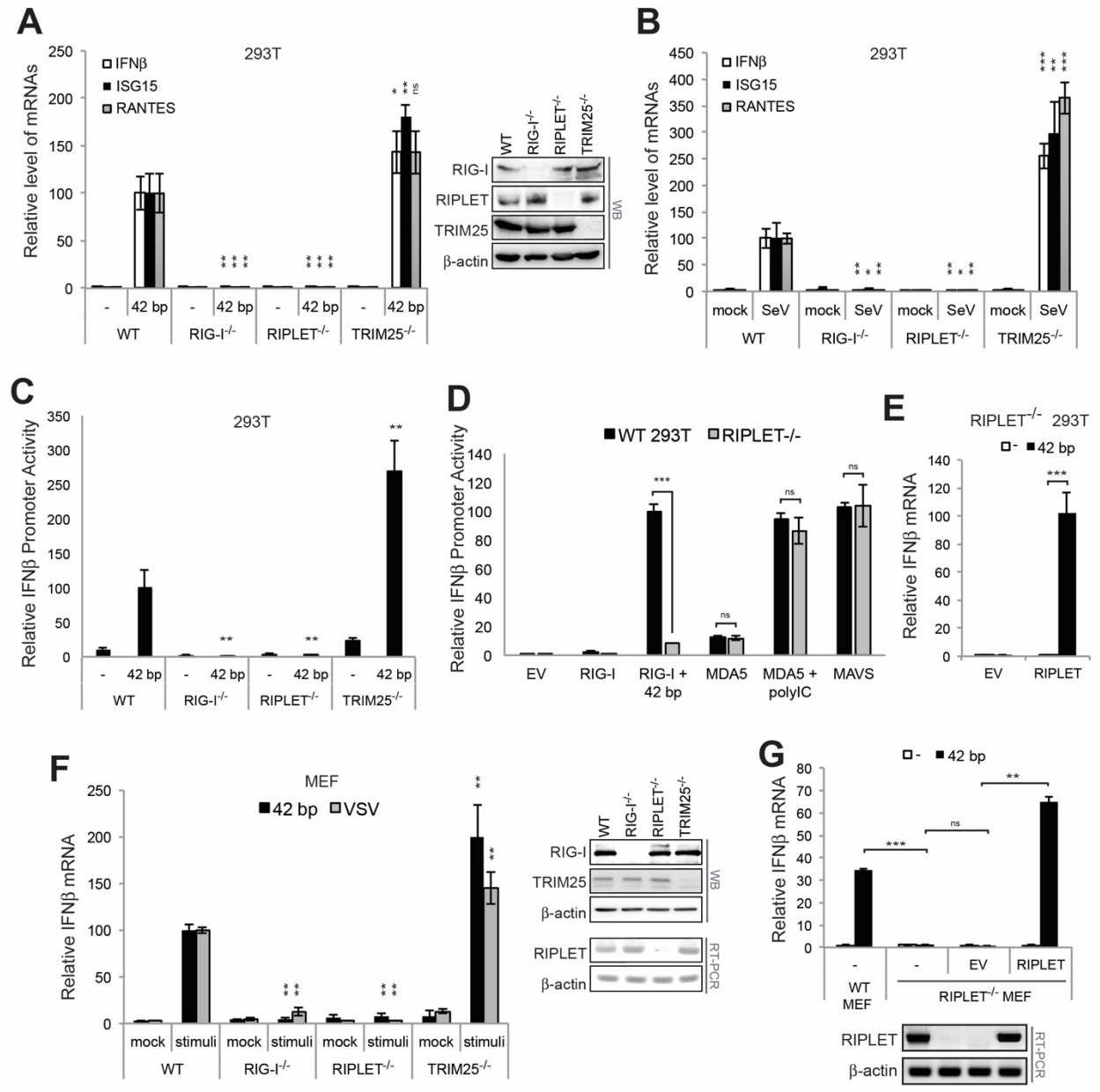

A
293T
IFNβ
ISG15
RANTES
Relative level of mRNAs
WT
RIG-I-/-
RIPLET-/-
TRIM25-/-
RIG-I
RIPLET
TRIM25
β-actin
WB
B
293T
mock
SeV
C
293T
Relative IFNβ Promoter Activity
D
WT 293T
RIPLET-/-
EV
RIG-I
RIG-I + 42 bp
MDA5
MDA5 + polyIC
MAVS
E
RIPLET-/- 293T
Relative IFNβ mRNA
F
MEF
42 bp
VSV
stimuli
RT-PCR
G
WT MEF
RIPLET-/- MEF

Figure 2.1 RIPLET, not TRIM25, is required for RIG-I signaling.

2.1A-B) Relative level of antiviral signaling in 293T cells (WT, RIG-I-/-, RIPLET-/- or TRIM25-/-), as measured by the level of IFN-β, ISG15 and RANTES mRNAs by qPCR. Unless mentioned otherwise, all RNAs used in this manuscript harbor 5'ppp. **2.1C)** Relative level of antiviral signaling in WT, RIG-I-/-, RIPLET-/- or TRIM25-/- 293T cells, as measured by the IFN-β promoter reporter assay. **2.1D)** Relative level of RIG-I, MDA5 and MAVS signaling in RIPLET-/- 293T cells. Cells were transfected with plasmid expressing RIG-I (10 ng), MDA5 (5 ng) or MAVS (25 ng), and were stimulated with 42 bp dsRNA (0.2 μg) or high molecular weight polyinosinic-polycytidylic acid (polyIC, 0.5 μg). Note that ectopic expression of MDA5 and MAVS is necessary to examine their signaling activities in 293T cells. RIG-I was ectopically expressed for comparison. The rest of Figure 2.1 measures the endogenous RIG-I activity. **2.1E)** Relative level of antiviral signaling in RIPLET-/- 293T cells with and without RIPLET complementation as measured by IFN-β qPCR. **2.1F)** Relative level of antiviral signaling in MEF cells (WT, RIG-I-/-, RIPLET-/- or TRIM25-/-), as measured by the level of IFN-β mRNA. Cells were stimulated with 42 bp dsRNA with 5'ppp (0.2 μg) or VSV (MOI=1). WB or RT-PCR analysis showing deletion of respective genes. For RIPLET, mRNA level was measured due to the lack of an appropriate antibody against mouse RIPLET. Note that the RIPLET WB in (A) is for human RIPLET. **2.1G)** Relative level of antiviral signaling in RIPLET-/- MEF cells with and without stable expression of RIPLET using lentivirus transduction.

All data are presented as mean ± s.d. (n = 3-4) and are representative of at least three independent experiments. * $p < 0.05$, ** $p < 0.01$, ***$p < 0.001$, ns, not significant (unpaired t test).

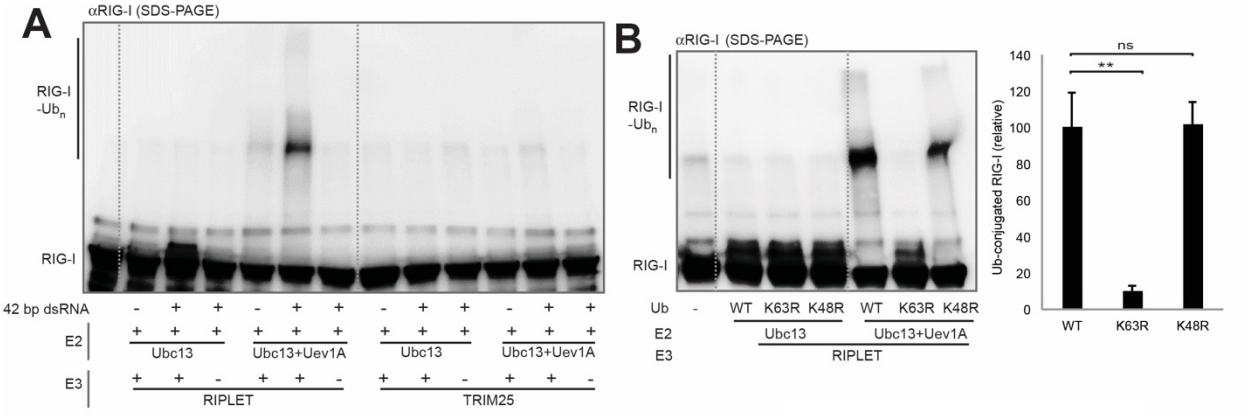
To further validate our observation, we examined additional knock-out cell lines from independent sources (Figures S1A-S1B). These included RIPLET-/- MEF from (Oshiumi et al., 2010) and TRIM25-/- MEF from (Gack et al., 2007). 5'ppp-dsRNA and VSV were used to stimulate RIG-I signaling. The dependence of RIG-I on RIPLET was confirmed in the independently generated RIPLET-/- MEF cell line (Figure S1A). A moderate reduction (~40 %) in RIG-I signaling was observed only with one of the TRIM25-/- MEF cell lines (Figure S1C). Note that the other TRIM25-/- cells showed little defect in RIG-I signaling (Figure 2.1), suggesting that the small defect in RIG-I signaling is specific to this cell line. Previous studies suggested that TRIM25 is required for the signaling activity of isolated 2CARD (Gack et al., 2007). In our analysis, TRIM25 knock-out led to ~50 % reduction in the signaling activity of GST-2CARD (Figure S1C). This result suggests that while TRIM25 is not necessary for full-length RIG-I signaling, it has a moderate stimulatory effect on the signaling activity of the isolated 2CARD. Note that the signaling activity of GST-2CARD was unaffected by RIPLET deletion (Figure S1C). The observed gain of TRIM25-dependence and the loss of RIPLET-dependence for GST-2CARD suggest that the signaling mechanism of GST-2CARD differs from that of full-length RIG-I.

2.4.2 RIPLET, not TRIM25, ubiquitinates RIG-I in a dsRNA-dependent manner

To test whether RIPLET or TRIM25 can directly conjugate K63-Ubn to RIG-I, we reconstituted the RIG-I ubiquitination reaction in vitro. A previous study showed that RIG-I signaling requires Ubc13 (i.e. Ube2N) (Shi et al., 2017), an Ub E2 conjugating enzyme that can function either by itself or in complex with catalytically inactive E2 variants, such as Uev1A (i.e. Ube2V1) (Wu and Karin, 2015). Incubation of RIG-I with purified E1, E2(s), and RIPLET showed that the Ubc13:Uev1A complex, but not Ubc13 alone, supported robust ubiquitination of RIG-I

(Figure 2.2A). Consistent with the lack of effect of RIPLET on MDA5 signaling, MDA5 was not ubiquitinated by RIPLET under the same condition (Figure S2A). The K63R mutation in Ub prevented polyUb chain conjugation by RIPLET (Figure 2.2B), suggesting that RIPLET primarily conjugates K63-Ubn to RIG-I. Although ubiquitinated RIG-I migrated into the SDS gel as a discrete band, it represents polyubiquitinated RIG-I (likely compressed in the resolving and stacking gel interface). This is evidenced by the appearance of smaller species when RIG-I was ubiquitinated with an increasing amount of the K63 chain terminator, K63R Ub (Figure 2.2C). Intriguingly, ubiquitination of RIG-I required presence of dsRNA (Figure 2.2A), recapitulating the cellular requirement of dsRNA for RIG-I signaling. Since RIPLET does not appear to bind dsRNA (Figure S2B), dsRNA-dependent ubiquitination suggests the specificity of RIPLET for the RIG-I:dsRNA complex over RNA-free RIG-I (to be confirmed in Figure 2.3).

Consistent with the non-essential role of TRIM25 for RIG-I signaling (Figures 2.1 and S1), no RIG-I ubiquitination was observed with TRIM25 under the equivalent condition (Figure 2.2A). While the lack of ubiquitination could be due to the use of inappropriate E2 enzymes, the Ubc13:Uev1A complex was found required for RIG-I signaling (Shi et al., 2017) and is so far the only cytosolic E2 known to synthesize K63-linked Ub chains, the linkage type required for 2CARD tetramerization (Peisley et al., 2014; Zeng et al., 2010). Under the same condition, TRIM25 robustly auto-ubiquitinated itself (Figure 2.2D), suggesting that purified TRIM25 is active.


A
αRIG-I (SDS-PAGE)
RIG-I -Ubn
RIG-I
42 bp dsRNA
E2
Ubc13
Ubc13+Uev1A
Ubc13
Ubc13+Uev1A
E3
RIPLET
TRIM25
B
αRIG-I (SDS-PAGE)
RIG-I -Ubn
RIG-I
Ub
WT K63R K48R WT K63R K48R
E2
Ubc13
Ubc13+Uev1A
E3
RIPLET
ns
**
Ub-conjugated RIG-I (relative)
140
120
100
80
60
40
20
0
WT
K63R
K48R

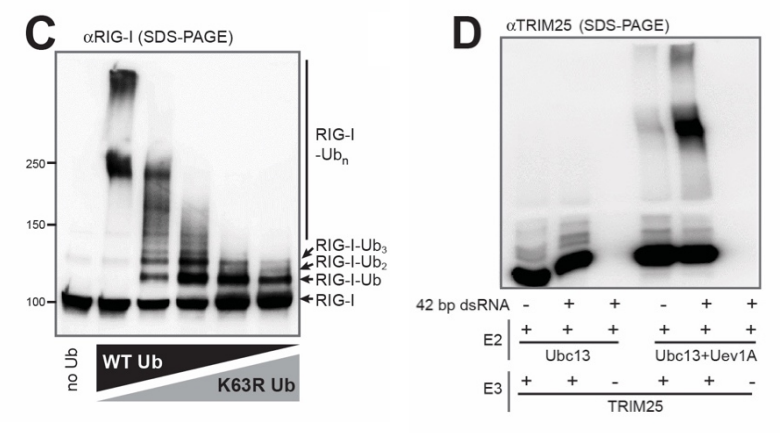

C
αRIG-I (SDS-PAGE)
250
150
100
RIG-I -Ubn
RIG-I-Ub3
RIG-I-Ub2
RIG-I-Ub
RIG-I
no Ub
WT Ub
K63R Ub
D
αTRIM25 (SDS-PAGE)
42 bp dsRNA
E2
Ubc13
Ubc13+Uev1A
E3
TRIM25

Figure 2.2: RIPLET, not TRIM25, ubiquitinates RIG-I in a dsRNA-dependent manner

2.2A) *In vitro* ubiquitination analysis of RIG-I. Purified E1 (1 μM), E2 (Ubc13 alone or in complex with Uev1A, 5 and 2.5 μM, respectably), E3 (RIPLET or TRIM25, 0.25 nM) and Ub (20 μM) were incubated with RIG-I (0.5 μM), either alone or in complex with 42 bp dsRNA (1 ng/μl). Ubiquitination of RIG-I was analyzed by anti-RIG-I blot on SDS gels. **2.2B)** RIG-I was ubiquitinated by RIPLET using Ub (WT, K63R or K48R) in the presence of 42 bp dsRNA. Right: quantitation of ubiquitinated RIG-I (mean ± s.d., n = 3). Ubiquitination reactions were performed as in (A). * $p < 0.05$, ** $p < 0.01$, ***$p < 0.001$, ns, not significant (unpaired t test, compared with WT Ub). **2.2C)** *In vitro* ubiquitination analysis of RIG-I in the presence of an increasing amount of K63R Ub (0, 25, 50, 75, 100%) mixed in with WT Ub. Total Ub concentration (20 μM) was kept constant. All reactions were performed in the presence of 42 bp dsRNA. **2.2D)** Analysis of TRIM25 auto-ubiquitination. Samples in Figure 2.2A were re-analyzed by anti-TRIM25 blot.

2.4.3 RIPLET recognizes pre-assembled RIG-I filaments on dsRNA

We next explored how RIPLET interacts with RIG-I and how this interaction depends on dsRNA. We purified recombinant RIPLET and RIG-I and used native gel shift assays to examine the mobility of fluorescently labeled RIG-I with and without RIPLET. Consistent with the dsRNA-dependent ubiquitination of RIG-I (Figure 2.2A), RIPLET bound RIG-I only in the presence of dsRNAs (Figure 2.3A). RIPLET did not bind MDA5 filaments (Figure S3A), consistent with its lack of a role in MDA5 signaling (Figure 2.1D) and ubiquitination (Figure S2A). The N-terminal 2CARD deletion mutant of RIG-I (RIG-IΔN) also bound RIPLET in a manner dependent on dsRNA. Isolated 2CARD did not bind RIPLET (Figure 2.3A), in agreement with the lack of effect of RIPLET on GST-2CARD signaling (Figure S1C). Further truncation of RIG-I to the helicase domain or CTD impaired RIPLET binding (Figure S3B), indicating that RIG-IΔN is minimally required. We then compared RIPLET binding to RIG-I in complex with 15, 21, 42, 62, and 162 bp dsRNAs, which can accommodate 1, 2, 3, 4-5 and 11-12 RIG-I molecules, respectively (Figure 2.3B). The mobility shift assay showed that RIPLET binding requires at least 21 bp dsRNA, i.e. two RIG-IΔN molecules in proximity.

RIPLET consists of the N-terminal RING, central coiled coil (CC) and C-terminal PSpry domains (Figure 2.3B). The RING domain is known to recognize E2 conjugating enzymes, and is essential for both RIG-I ubiquitination and unanchored Ubn synthesis (Figure S3D). RING deletion (ΔRING) had little impact on RIG-I binding (Figure 2.3B), consistent with the role of RING in E2 engagement rather than substrate binding. Further deletion of the CC domain, however, abolished RIG-I binding (Figure 2.3C). Since CC is responsible for dimerization of RIPLET (Figure S3D), we examined the importance of dimerization by replacing CC by an

orthogonal dimeric protein, GST. The GST-PSpry fusion fully restored RIG-I binding (Figures 2.3C and S3E), suggesting that PSpry is the RIG-I binding domain, and bivalency is required for high affinity binding (Figure 2.3D). This is in line with the observation that RIPLET binds RIG-I only in complex with dsRNA that is long enough to accommodate at least two RIG-I molecules (Figure 2.3B).

We next explored how the bivalent binding mode of RIPLET affects dsRNA length selectivity of RIG-I. We expected that RIPLET would bind and ubiquitinate RIG-I filaments on longer dsRNA more efficiently, because longer filaments would allow many more RIPLET binding configurations (Figure 2.3D). Comparison of the ubiquitination efficiency, however, showed that RIPLET ubiquitinates RIG-I most efficiently when RIG-I is bound with ~30-40 bp dsRNAs. This ubiquitination is more efficient than when RIG-I is bound with >40 bp dsRNAs (Figure 2.3E). Although RIG-I filament formation is known to be limited on >~0.5-1 kb dsRNAs (because the filament assembles from a dsRNA end and its propagation to the dsRNA interior is relatively inefficient, Peisley et al., 2013), which could partly explain the decline in Ub conjugation with ~500 bp dsRNA, the maximum ubiquitination at ~30-40 bp was unexpected given the efficient RIG-I filament formation on ~40-~200 bp dsRNA (Binder et al., 2011; Peisley et al., 2013). The inefficient ubiquitination of RIG-I on >~40 bp RNAs and its preference for longer dsRNAs in RIG-I signaling led us to question whether RIPLET binds RIG-I differently on >~40 bp dsRNA, perhaps in a manner conducive to RIG-I signaling, but not for ubiquitination. Intriguingly, with longer dsRNAs, we observed two populations of RIG-I:RIPLET complexes in native gels: those migrating into the gel and those remaining in the gel well (Figure S3F)

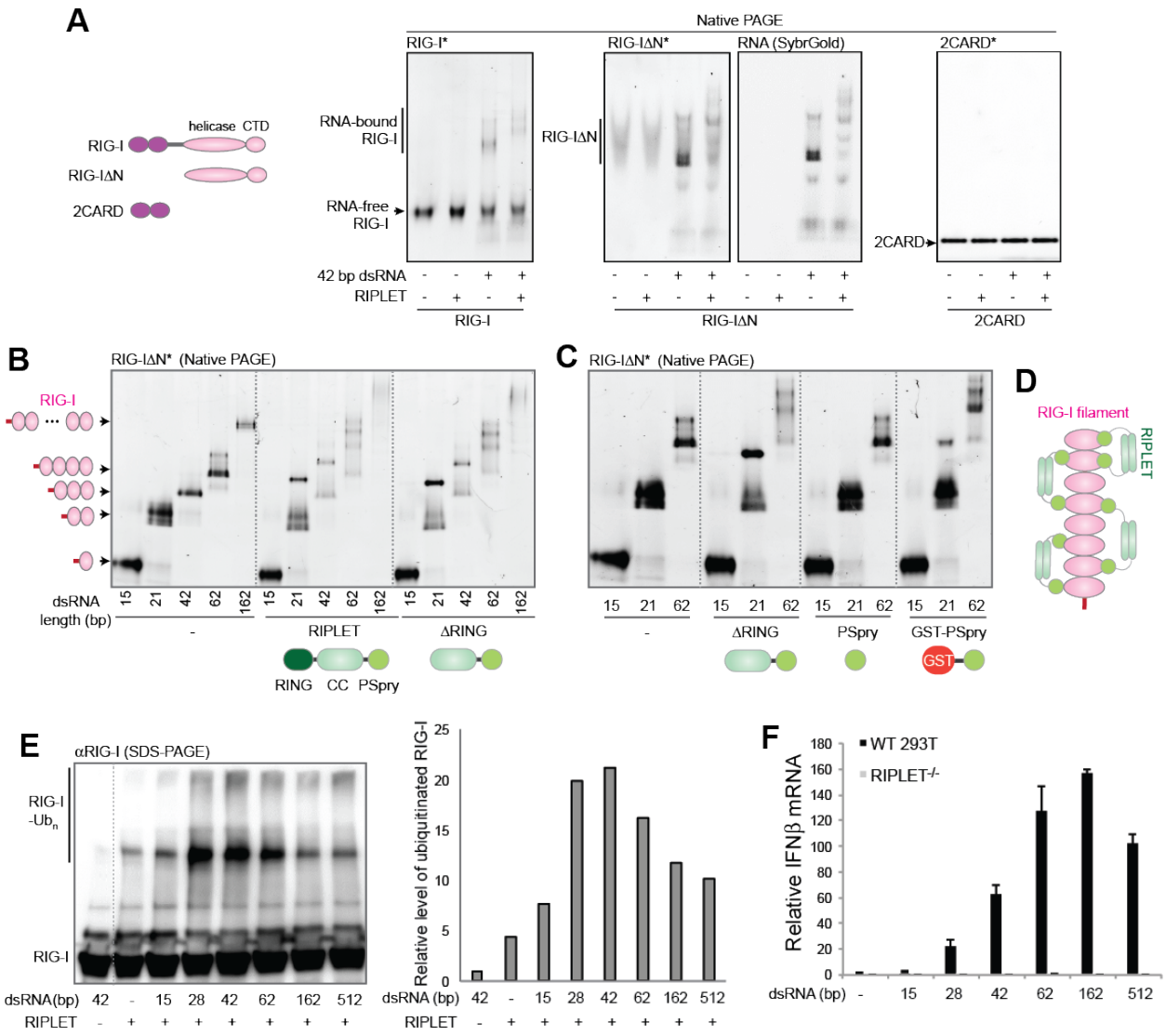

A
Native PAGE
RIG-I*
RIG-IΔN*
RNA (SybrGold)
2CARD*
helicase CTD
RIG-I
RIG-IΔN
2CARD
RNA-bound RIG-I
RNA-free RIG-I
RIG-IΔN
2CARD
42 bp dsRNA
RIPLET
RIG-I
RIG-IΔN
2CARD
B
RIG-IΔN* (Native PAGE)
RIG-I
dsRNA length (bp)
15 21 42 62 162
RIPLET
ΔRING
RING CC PSpry
C
RIG-IΔN* (Native PAGE)
15 21 62
ΔRING
PSpry
GST-PSpry
GST
D
RIG-I filament
RIPLET
E
αRIG-I (SDS-PAGE)
RIG-I -Ub$_n$
RIG-I
dsRNA(bp) 42 - 15 28 42 62 162 512
RIPLET
Relative level of ubiquitinated RIG-I
F
WT 293T
RIPLET$^{-/-}$
Relative IFNβ mRNA
dsRNA (bp) - 15 28 42 62 162 512

Figure 2.3: RIPLET recognizes pre-oligomerized RIG-I on dsRNA and activates RIG-I signaling in a dsRNA length-dependent manner

2.3A) Native gel shift assay to monitor the interaction between RIG-I and RIPLET. Fluorescently labeled RIG-I (full-length RIG-I, RIG-IΔN or isolated 2CARD, 0.5 μM) was incubated with RIPLET (0.5 μM) in the presence or absence of 42 bp dsRNA (1 ng/μl). The complex was analyzed by native gel using RIG-I fluorescence (*). For RIG-IΔN, SybrGold stained image was also shown to clearly visualize only the RNA-bound species. **2.3B-C)** Native gel shift assay of RIG-IΔN (0.5 μM) with and without RIPLET (B), ΔRING (B, C), PSpry (C) or GST-PSpry (C) (0.5 μM for all RIPLET variants). 15-162 bp dsRNAs (1 ng/μl) were used to form the RIG-I:dsRNA complexes of various sizes. Gel images were acquired using RIG-I fluorescence (*). **2.3D)** A model of how RIPLET binds RIG-I filaments. Based on the dsRNA length dependence and bivalency requirement, we propose that RIPLET binds two nearby RIG-I monomers within a filament (either immediately adjacent or separated). The lengths of RIPLET CC (~60 amino acids, expected to be ~80 Å) and the linker between CC and PSpry (~50 amino acids, expected to be >100 Å for fully disordered linker) are compatible with the model. **2.3E)** In vitro ubiquitination analysis of RIG-I in the presence of 15-512 bp dsRNAs (1 ng/μl for all RNAs). Right: densitometry analysis of ubiquitinated RIG-I, representative of three independent analyses. Anti-RIG-I immunoblot was used for quantitation. A similar dsRNA length-dependence was observed by fluorescence measurement using FITC-labeled RIG-I. **2.3F)** Relative level of antiviral signaling in response to 15-512 bp dsRNA (0.2 μg for all RNAs) in 293T cells (WT or RIPLET-/-), as measured by the IFN-β mRNA level (mean ± s.d., n = 3). All data are representative of at least three independent experiments.

2.4.4 RIPLET cross-bridges RIG-I filaments *in vitro*

To examine how RIPLET binds RIG-I filaments on long dsRNAs and whether RIPLET can induce additional higher-order oligomerization of RIG-I, we employed negative stain EM to visually inspect the RIPLET:RIG-I complex. We chose 162 bp and 512 bp dsRNAs, the two longest dsRNAs used in Figure 2.3. Consistent with previous findings (Peisley et al., 2013), RIG-I formed filaments only upon dsRNA binding (Figures 2.4A and S4A). Note that dsRNA alone or RIG-I alone are generally invisible by negative stain EM because of inefficient staining and small sizes. This allows clear identification of RIG-I filaments on dsRNA. Comparison of RIG-I filaments before and after RIPLET addition showed that RIPLET induces RIG-I filament bridging (Figure 2.4A). This was observed with both162 bp and 512 bp dsRNAs. Similar to the intra-filament binding mode, filament bridging required neither the RING domain of RIPLET (Figure 2.4A) nor the 2CARD domain of RIG-I (Figure 2.4B). No such aggregate structure was found in the absence of dsRNA or RIG-I (Figure 2.4B). RIPLET also did not bridge MDA5 filaments (Figure S4B), consistent with the specificity of RIPLET for RIG-I, not MDA5 (Figure 2.1D & S3B).

To independently examine the filament bridging activity, we developed a biotin-RNA pull-down assay, in which the association between biotinylated and non-biotinylated dsRNAs was examined in the presence and absence of RIG-IΔN and RIPLETΔRING (Figure 2.4C). RIG-IΔN and ΔRING were incubated with a mixture of 3'-biotinylated 112 bp dsRNA and non-biotinylated dsRNA of 162 bp. Biotin-dsRNA and the bound proteins were purified with streptavidin beads, and the level of co-purified, non-biotinylated dsRNA was analyzed by gel. In the absence of RIPLET, co-purification of 162 bp dsRNA and biotin-112 bp dsRNA was minimal and was not improved by the addition of RIG-IΔN (Figure 2.4C). In fact, RIG-IΔN negatively

affected purification of biotin-112 bp dsRNA (Figure 2.4C), which is likely due to the reduced accessibility of the 3'-conjugated biotin moiety upon RIG-I binding to the dsRNA end. In the presence of ΔRING, however, 162 bp dsRNA was co-purified with biotin-112 bp dsRNA only in the presence of RIG-IΔN (Figure 2.4C). PSpry did not promote dsRNA co-purification. The requirement of ΔRING and RIG-IΔN for dsRNA co-purification is consistent with the filament bridging activity of RIPLET. Furthermore, comparison of the recovery rate of non-biotinylated 21-512 bp dsRNAs showed that dsRNA co-purification is more efficient with longer dsRNAs (Figure 2.4D), as would be expected for filament bridging.

To further examine how ΔRING bridges RIG-I filaments, we tested the bridging activity of GST-PSpry, which binds RIG-I filaments as efficiently as ΔRING (Figure S3E). Intriguingly, GST-PSpry did not promote RIG-I filament bridging as measured by both EM and biotin-RNA pull-down assay (Figures 2.4E and 2.4F). This result suggests that RIPLET CC is important for RIG-I filament bridging and its role is beyond simple dimerization. Considering that RIPLET CC, but not GST, can bridge RIG-I filaments, we speculate that long antiparallel dimeric CCs may have weak affinity for each other. This weak interaction may stabilize when RIPLET is locally concentrated on a RIG-I filament, resulting in the formation of multivalent RIPLET oligomers and bridging of RIG-I filaments (Figure 2.4G).

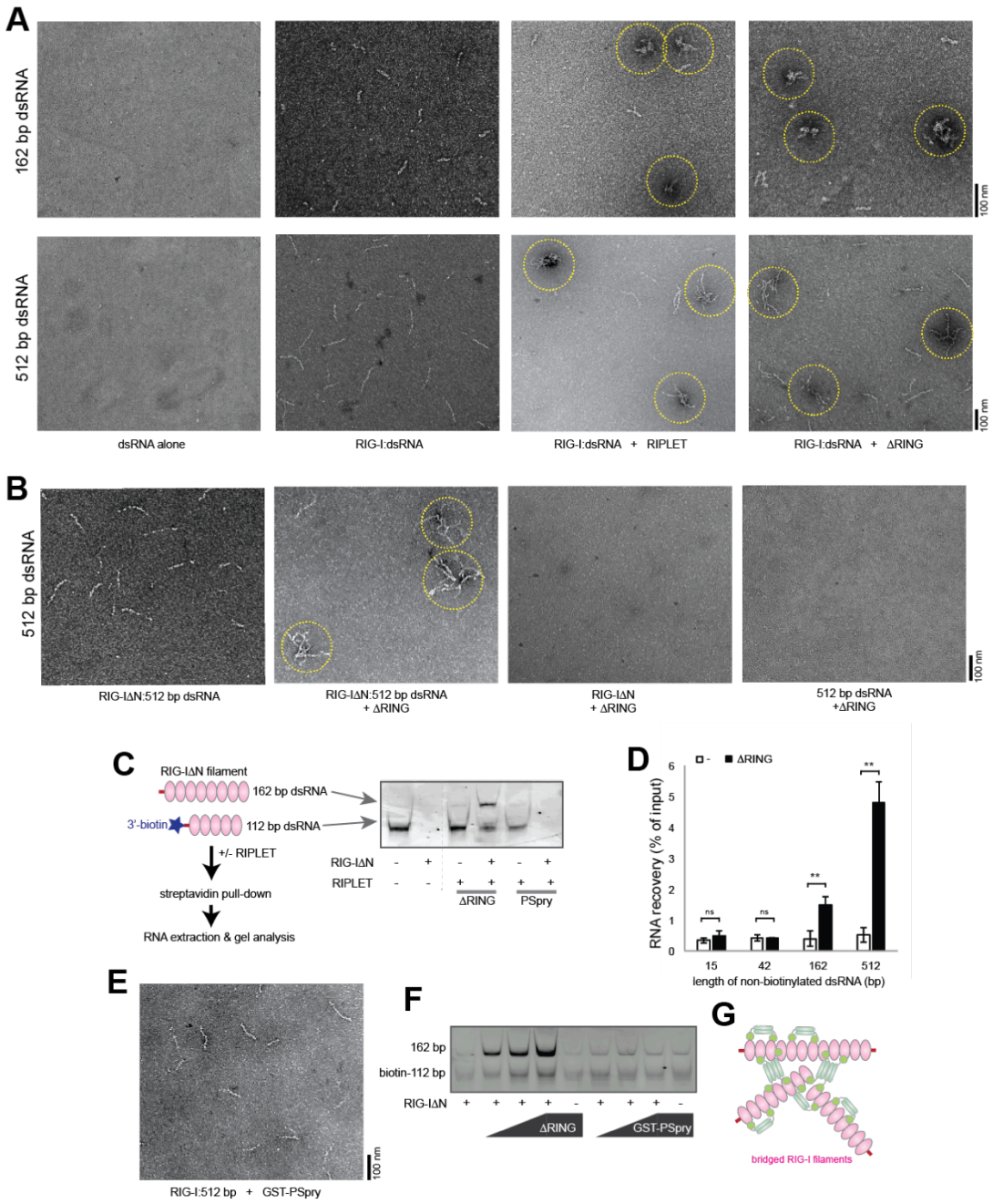

A
162 bp dsRNA
512 bp dsRNA
100 nm
dsRNA alone
RIG-I:dsRNA
RIG-I:dsRNA + RIPLET
RIG-I:dsRNA + ΔRING
B
512 bp dsRNA
RIG-IΔN:512 bp dsRNA
RIG-IΔN:512 bp dsRNA + ΔRING
RIG-IΔN + ΔRING
512 bp dsRNA +ΔRING
C
RIG-IΔN filament
162 bp dsRNA
3'-biotin
112 bp dsRNA
+/- RIPLET
streptavidin pull-down
RNA extraction & gel analysis
RIG-IΔN
RIPLET
ΔRING
PSpry
D
- ΔRING
RNA recovery (% of input)
ns
**
15
42
162
512
length of non-biotinylated dsRNA (bp)
E
RIG-I:512 bp + GST-PSpry
F
162 bp
biotin-112 bp
RIG-IΔN
ΔRING
GST-PSpry
G
bridged RIG-I filaments

Figure 2.4: RIPLET cross-bridges RIG-I filaments *in vitro*

2.4A) Representative EM images of RIG-I filaments (0.5 μM) formed on 162 bp (top) or 512 bp (bottom) dsRNA (1 ng/μl), in the presence and absence of RIPLET or ΔRING (0.5 μM). Cross-bridged RIG-I filaments are highlighted with yellow circles. **2.4B)** Representative EM images of RIG-IΔN filaments (0.5 μM) formed on 512 bp dsRNA (1 ng/μl), in the presence or absence of ΔRING (0.5 μM). Images for ΔRING incubated with RIG-IΔN alone or dsRNA alone were shown on the right as controls. **2.4C)** Streptavidin pull-down analysis to examine RIPLET-mediated cross-bridging of RIG-I filaments. RIG-IΔN filaments (0.5 μM) were formed on non-biotinylated 162 bp dsRNA (1 ng/μl) and 3'-biotinylated 112 bp dsRNA (1 ng/μl), and the complexes were incubated with ΔRING prior to streptavidin pull-down. The bound RNA was extracted and analyzed by native PAGE (right). **2.4D)** Recovery rate (mean ± s.d., n = 3) of non-biotinylated 21-512 bp dsRNA (1 ng/μl) when incubated with 3'-biotinylated 112 bp dsRNA (1 ng/μl) and RIG-IΔN in the presence and absence of ΔRING, as in (C). * $p < 0.05$, ** $p < 0.01$, ns, not significant (unpaired t test, compared with no ΔRING). **2.4E)** Representative EM image of RIG-I filaments (0.5 μM) formed on 512 bp dsRNA (1 ng/μl), in the presence of GST-PSpry (0.5 μM). **2.4F)** Streptavidin pull-down analysis using an increasing concentration of ΔRING or GST-PSpry (0.25, 0.5, and 1 μM). The experiment was performed as in (C). **2.4G)** A model of how RIPLET cross-bridges RIG-I filaments. Weak inter-dimeric interactions between coiled coils (CCs) may allow RIPLET to form multi-valent oligomers (tetramer or larger species) when clustered on a RIG-I filament. Multi-valent RIPLET oligomers would then allow cross-bridging of distinct RIG-I filaments. Note that the two RIPLET binding modes, intra-filament binding (in Figure 2.3D) and inter-filament bridging, are not mutually exclusive and can co-occur on the same RIG-I filament.

2.4.5 RIPLET cross-bridges RIG-I filaments in cells independent of stress granules (SGs)

To further examine whether RIPLET-mediated bridging of RIG-I filaments indeed occurs in cells, we performed a similar biotin-RNA pull-down analysis in WT and RIPLET-/- 293T cells. Upon transfection with biotin-112 bp dsRNA and non-biotinylated 162 bp dsRNA, cells were lysed and subjected to streptavidin pull-down. The level of 162 bp dsRNA co-purified with biotinylated RNA was measured by RT-qPCR. The result showed that 162 bp dsRNA was co-purified in a manner dependent on biotinylated 112 bp dsRNA (Figure 2.5A). More importantly, co-purification of 112 bp and 162 bp dsRNA was impaired by RIPLET knock-out (Figure 2.5A) and was restored by ΔRING complementation (Figure 2.5B). Similarly, non-biotinylated 512 bp dsRNA was co-purified with biotinylated 112 bp in an RIPLET-dependent manner (Figures 2.5A & 2.5B). These data suggest that RIPLET bridges RIG-I filaments in cells and at the endogenous level of RIG-I and RIPLET. Note that the observed co-purification of dsRNAs is independent of stress granules (SGs). SGs are cytosolic phase separation structures formed by RNA and RNA-binding proteins including RIG-I (Oh et al., 2016; Onomoto et al., 2013), and are known to form upon dsRNA stimulation (Figure 2.5C). In the absence of CHX, we still observed RIPLET-dependent RNA bridging, but the use of CHX significantly reduced the background RNA bridging (Figure 2.5D). Note that Figures 2.5A-B were performed in the presence of CHX (see the flow chart in Figure 2.5A). The observed co-purification of two RNAs, even in the presence of CHX, suggests that RIPLET-mediated filament bridging occurs independent of SGs. CHX also did not negatively affect RIG-I signaling (Figure 2.5E), suggesting that SG localization of RIG-I, which is distinct from RIPLET-mediated filament bridging, is not important for antiviral signaling. The role of recruitment of RIG-I into SGs will be further explained in chapter 3 of this work (below).

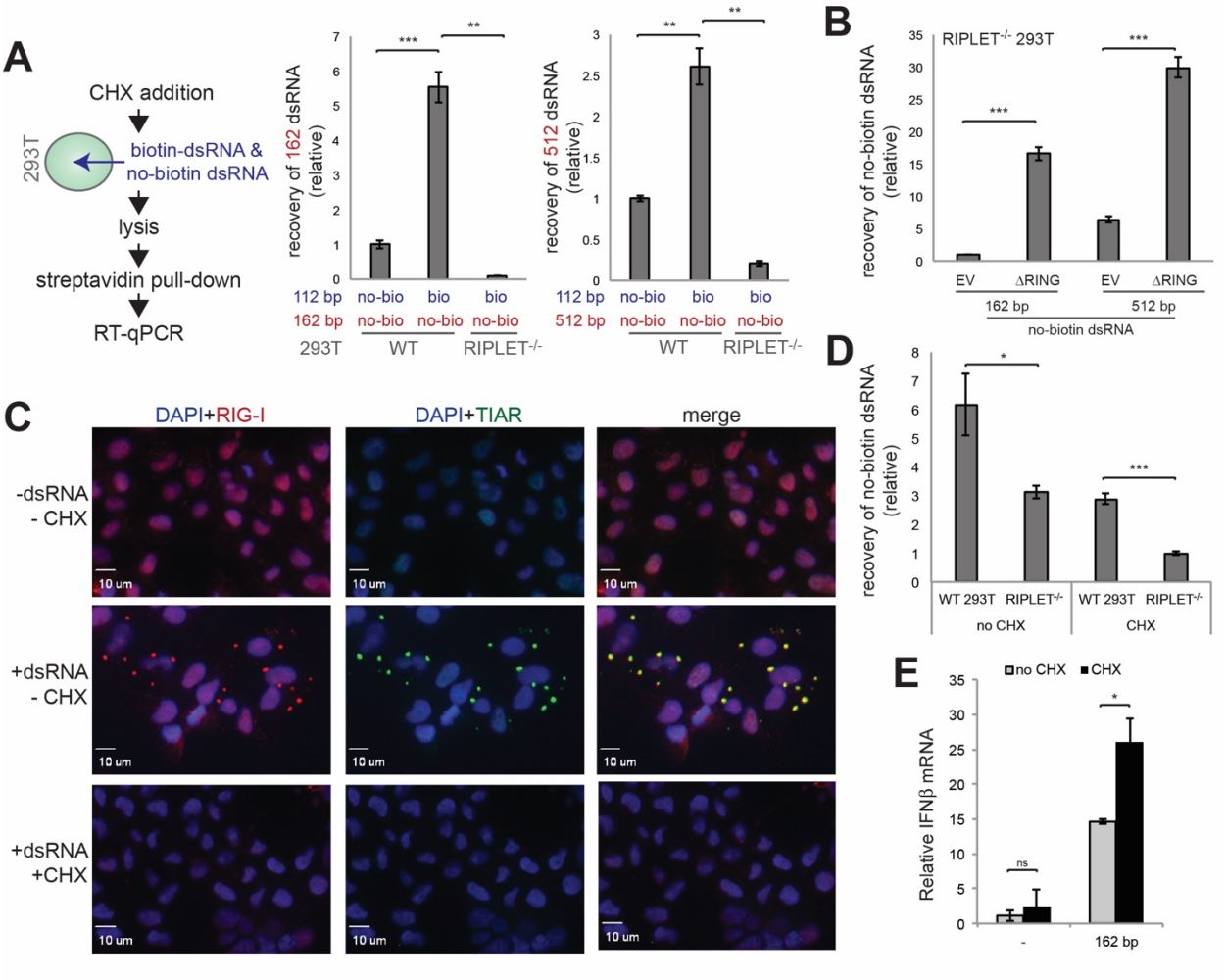

A
CHX addition
293T
biotin-dsRNA &
no-biotin dsRNA
lysis
streptavidin pull-down
RT-qPCR
recovery of 162 dsRNA (relative)
recovery of 512 dsRNA (relative)
112 bp
162 bp
512 bp
no-bio
bio
293T
WT
RIPLET-/-
B
RIPLET-/- 293T
recovery of no-biotin dsRNA (relative)
EV
ΔRING
162 bp
512 bp
no-biotin dsRNA
C
DAPI+RIG-I
DAPI+TIAR
merge
-dsRNA
- CHX
+dsRNA
- CHX
+dsRNA
+CHX
10 um
D
recovery of no-biotin dsRNA (relative)
WT 293T
RIPLET-/-
no CHX
CHX
E
no CHX
CHX
Relative IFNβ mRNA
ns
-
162 bp

Figure 2.5: RIPLET cross-bridges RIG-I filaments in cells independent of stress granules

2.5A) *In cellulo* strepavidin pull-down analysis. WT and RIPLET-/- 293T cells were treated with cyclohexamide (CHX, 0.1 mg/ml) an hour before transfection with non-biotinylated dsRNA (either 162 bp or 512 bp, 1 μg in a 6 well plate) and 3'-biotinylated 112 b dsRNA (1 μg). Cells were lysed 4 hrs post RNA transfection and were subjected to streptavidin pull-down as described in STAR methods. Co-purification of non-biotinylated 162 bp or 512 bp dsRNA was measured by RT-qPCR. No-bio and bio refer to non-biotinylated dsRNA and biotinylated dsRNA, respectively. **2.5B)** *In cellulo* strepavidin pull-down analysis using 162/512 bp dsRNA (1 μg) and 3'-biotinylated 112 bp dsRNA (1 μg). The ΔRING construct (or empty vector, EV) was transfected into RIPLET-/- 293T cells 24 hr before dsRNA transfection. **2.5C)** Immunofluorescence analysis of endogenous RIG-I and SGs (marked by TIAR staining) in 293T cells in the presence and absence of 162 bp dsRNA (0.5 μg) and CHX. Cells were treated with CHX (0.1 mg/ml) an hour before transfection with dsRNA, and fixed for imaging 2 hr post dsRNA transfection. **2.5D)** *In cellulo* strepavidin pull-down analysis with and without CHX (0.1 mg/ml). **2.5E)** The effect of CHX (0.1 mg/ml) on RIG-I signaling in response to 162 bp dsRNA.

All data are presented as mean ± s.d. (n = 3 for A-D and n = 2 for E) and are representative of three independent experiments. * $p < 0.05$, ** $p < 0.01$, ***$p < 0.001$, ns, not significant (unpaired t test).

2.4.6 RIG-I signaling is enhanced by RIPLET-mediated filament cross-bridging

We next asked whether filament bridging contributes to RIG-I signaling. On one hand, filament bridging would cluster RIG-I molecules, which could promote 2CARD tetramerization and thus, MAVS activation, with or without K63-Ubn. On the other hand, SG assembly, which also clusters RIG-I in a RIPLET-independent manner, had no impact on RIG-I signaling (Figure 2.5E). To test the effect of RIG-I filament bridging in cells, we compared the RIG-I-stimulatory activity of full-length RIPLET and RING fused to GST-PSpry (RING-GST-PSpry) in RIPLET-/- 293T cells. RIPLET can bridge RIG-I filaments, while GST-PSpry cannot (Figures 2.4E-F). The result shows that RIPLET is a more potent stimulator of RIG-I than is RING-GST-PSpry (Figure 2.6A), consistent with the notion that RIG-I filament bridging stimulates RIG-I signaling. Furthermore, ΔRING, which can bridge RIG-I filaments but cannot ubiquitinate RIG-I (Figures 2.4A & S3C), also enhanced RIG-I signaling in response to dsRNA and viral infection (Figures 2.6B & 2.6C), albeit not as efficiently as full-length RIPLET. The RIG-I-stimulatory effect of ΔRING was observed with both transiently expressed ΔRING (Figures 2.6B & 2.6C) and stably reconstituted ΔRING (Figure S6A). Furthermore, comparison among dsRNAs of various lengths suggests that ΔRING-mediated RIG-I signaling is more pronounced with longer RNA (Figure 2.6D), consistent with the length-dependence of filament bridging. While the exact pattern of dsRNA length dependence in Figure 2.6D differs from that of in vitro filament bridging in Figure 2.4D, this is likely because the latter is the measure of RNA bridging, not the level of RIG-I clustering and its impact on signaling. Altogether, these observations collectively support the notion that RIPLET uses the filament bridging activity to amplify RIG-I signaling and this activity synergizes with the Ub-dependent RIG-I stimulatory activity.

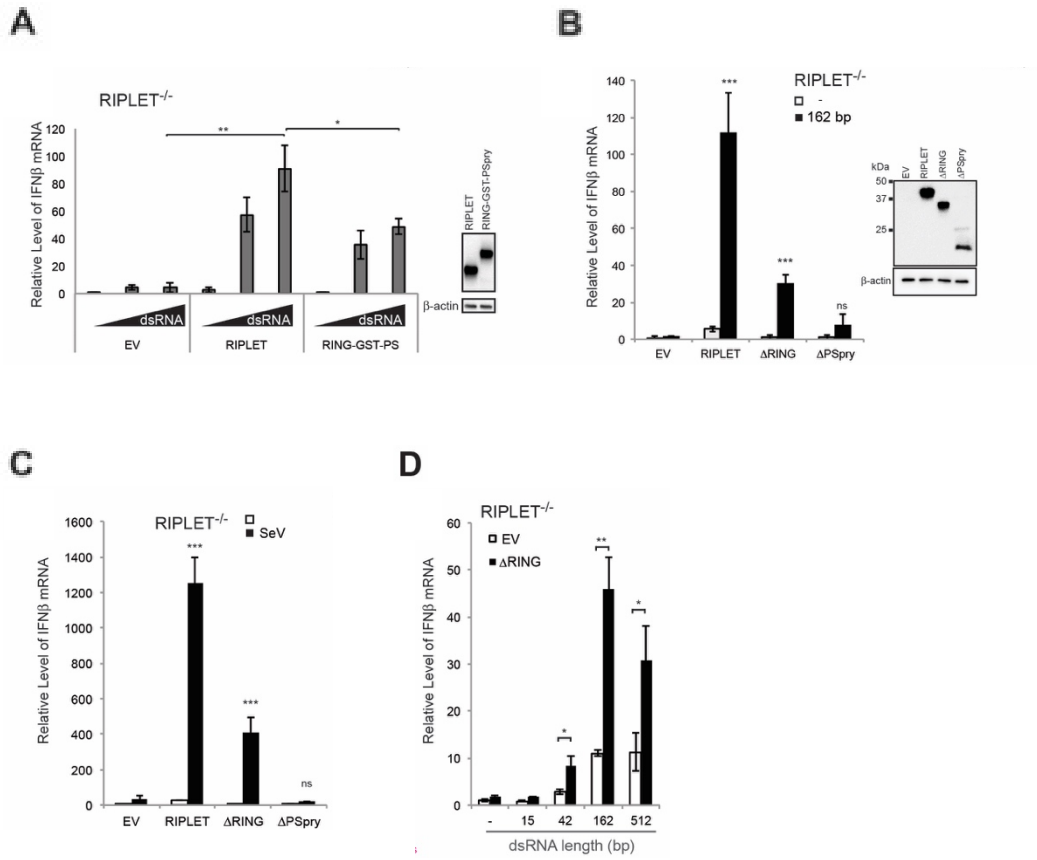


Figure 2.6: RIPLET-mediated RIG-I aggregation enhances antiviral signaling, in both ubiquitin-dependent and -independent manners.

2.6A) Comparison between full-length RIPLET and RING fused to GST-PSpry (RING-GST-PSpry) (20 ng each) in the RIG-I stimulatory activity. Relative level of antiviral signaling was measured upon stimulation with 162 bp dsRNA (0.2 μg) in RIPLET-/- 293T.

2.6B-C) Relative level of RIG-I signaling upon stimulation with 162 bp dsRNA (0.2 μg) (B) or SeV (100 HA units/ml) (C) in RIPLET-/- 293T cells complemented with empty vector (EV), RIPLET, ΔRING or ΔPSpry (20 ng). The level of antiviral signaling was measured by IFN-β mRNA. All cells were transiently transfected with the RIG-I expression plasmid (10 ng). See Figure S6 for the effect of ΔRING on endogenous RIG-I. **2.6D)** dsRNA length-dependence of the effect of ΔRING on RIG-I signaling.

2.5 Discussion

According to the current notion in the field of RIG-I signaling, RIG-I is activated by dsRNA binding and subsequently by TRIM25-mediated ubiquitination. This was largely based on the studies of isolated 2CARD, the signaling domain of RIG-I. RIPLET was later identified as a required protein for RIG-I signaling, but was shown to lack the stimulatory effect on isolated 2CARD (Gao et al., 2009; Oshiumi et al., 2009; Oshiumi et al., 2010). Based on the signaling activity of isolated 2CARD, which partially depends on TRIM25 but not on RIPLET, RIPLET was proposed to function upstream of TRIM25 in releasing the auto-repression of 2CARD (Oshiumi et al., 2013). We here showed that RIPLET, but not TRIM25, is required for full-length RIG-I signaling (Figures 1 and S1), and that the mode of action of RIPLET differs from what was previously proposed. While we did observe a moderate (~2-fold) stimulatory effect of TRIM25 on the signaling activity of isolated RIG-I 2CARD, as previously reported (Gack et al., 2007) (Figures S1H & S1I), knocking-out TRIM25 had little negative impact on full-length RIG-I signaling (Figures 1 and S1). This was demonstrated using multiple, independent knock-out cell lines in two different cell types (293T and MEF) with three different RIG-I stimuli (dsRNA, SeV, and VSV). The lack of impact of TRIM25 on RIG-I function was surprising given the widely held view of its essential role in RIG-I signaling. Considering the growing list of RIG-I-independent functions of TRIM25 in antiviral immunity–in part mediated by its RNA binding activity (Choudhury et al., 2014; Manokaran et al., 2015; Meyerson et al., 2017) and its interaction with ZAP (Li et al., 2017; Zheng et al., 2017)–the precise nature of the observed effect of TRIM25 on RIG-I 2CARD requires more detailed investigation.

Using a combination of biochemical analyses, we also showed that RIPLET is sufficient to conjugate full-length RIG-I with K63-Ub_n (Figure 2.2). TRIM25 does not ubiquitinate full-length RIG-I as robustly as RIPLET (Figure 2.2A). While previous studies, including previous studies in from lab (Peisley et al., 2014), described ubiquitination of isolated 2CARD by TRIM25, this required significantly higher concentrations of E1, E2, E3 enzymes and substrates. More importantly, ubiquitination of RIG-I by TRIM25 is not stimulated by dsRNA (Figure 2.2A), further raising a question on the role of TRIM25 in RIG-I ubiquitination. By contrast, RIPLET binds and ubiquitinates RIG-I only upon dsRNA binding (Figures 2.2 and 2.3), the mode of action consistent with the cellular activation condition for RIG-I signaling.

Our biochemical analyses of RIPLET revealed a novel mechanism by which RIPLET recognizes RIG-I in an oligomeric state-specific manner, and further induces higher order receptor "clustering". RIPLET binds the core RIG-I filaments formed by the helicase domain and CTD, and ubiquitinates multiple sites on the RIG-I protein, including 2CARD. More detailed analysis of the interactions between RIPLET and RIG-I showed that RIPLET utilizes its dimeric structure and the bivalent binding mode to preferentially recognize and ubiquitinate filamentous oligomers of RIG-I on >20 bp dsRNA. On longer dsRNA, RIPLET can also cross-bridge RIG-I filaments in an Ub-independent manner. This bridging further promotes the signaling activity of RIG-I, likely by inducing high local concentrations of the receptor, thereby facilitating 2CARD tetramerization. The combination of the intra-filament binding and inter-filament bridging modes enables RIG-I to signal more efficiently on longer dsRNA. In other words, RIPLET utilizes both Ub-dependent and –independent mechanisms to amplify RIG-I signaling on the basis of dsRNA length.

Based on the role of RIPLET in both RNA-discrimination and receptor oligomerization, we propose that RIPLET functions more like a co-receptor, rather than a downstream accessory protein. Our findings on RIPLET provide a previously unrecognized mechanism for how the innate immune system utilizes an E3 ligase to measure foreign nucleic acid length, a criterion commonly used by DNA and RNA sensors for self vs. non-self discrimination (Andreeva et al., 2017; Morrone et al., 2014; Peisley et al., 2012; Zhou et al., 2018). Additionally, RIPLET-mediated clustering of RIG-I provides a new perspective on receptor clustering, a phenomenon studied primarily in the context of cell-surface receptors (Hartman and Groves, 2011). It is yet unclear exactly how RIPLET specifically recognizes RIG-I filaments and discriminates against MDA5 filaments. Considering that a viral protein can distinguish between RIG-I and MDA5 using a single amino acid difference (Motz et al., 2013; Rodriguez and Horvath, 2013), one could speculate an analogous, sequence-dependent recognition mechanism for RIPLET. Future research is required to understand how RIPLET specifically recognizes RIG-I, and which E3 ligase recognizes MDA5 and how. Given the importance of the coiled-coil dimeric architecture in RIPLET functions and the commonality of this architecture in many E3 ligases (e.g. TRIM family members), our findings on RIPLET may be widely applicable to other E3 ligases recognizing MDA5 and beyond.

Chapter 3:

Resolution of RIG-I Signaling Aggregates in Antiviral Immunity

Author Contributions:

Cadena C and Hur S designed experiments and analyzed data. CC performed experiments.

3.1 Abstract

Efficient host defense against viral infection depends on the proper function of pattern recognition receptors. RIG-I is a pattern recognition receptor that senses viral dsRNA during infection. Previously, we investigated the early steps in the activation of RIG-I that lead to the induction of an IFN response. Specifically, we uncovered the molecular mechanism by which RIG-I and its co-receptor, the E3 ligase RIPLET, form aggregate-like assemblies. These aggregate-like assemblies are required for the induction of innate immune signaling. However, the process by which these macromolecular assemblies are resolved following signaling remains poorly understood. We and others have shown that dsRNA stimulation induces the recruitment of RIG-I and other signaling molecules into atypical stress granules (SGs). Here, I will present findings about the role of SGs in the resolution of macromolecular signaling complexes.

3.2 Introduction

RIG-I is a critical cytoplasmic sensor of viral double stranded RNA (dsRNA). In sterile conditions, RIG-I remains in an auto-inhibited state wherein the CARD signaling domain is secluded within the protein (Kowalinski et al., 2011). Upon infection, RIG-I binds the viral dsRNA and releases its CARD signaling domain, which then interacts with the CARD domain of the immediate downstream signaling adaptor MAVS (Kowalinski et al., 2011; Rawling et al., 2015; Jiang et al., 2012). The interaction between RIG-I CARD and MAVS requires the assembly of a CARD tetramer (Peisley et al., 2014). The activation RIG-I and its robust signaling depend on both dsRNA binding and the assembly of large molecular weight signaling complexes (reviewed in Cadena and Hur, 2019). RIG-I first binds the dsRNA end as a monomer, but then uses ATP hydrolysis to translocate to the interior of the dsRNA (Binder et al., 2011; Devarkar et al., 2018; Myong et al., 2009; Patel et al., 2013; Peisley et al., 2013). Repeating the process of end-binding and translocation leads to 'coating' of the dsRNA length by RIG-I molecules (Peisley et al., 2013). More recently, we described an additional layer of RIG-I aggregation mediated by the ubiquitin ligase RIPLET (Cadena et al., 2019). RIPLET has an antiparallel dimeric structure that allows it to bind RIG-I filaments at both ends of the dimer, leading to cross-bridging of RIG-I filaments. Both RIG-I filament formation and RIPLET-mediated filament bridging promotes RIG-I signaling by concentrating CARD domains available for CARD tetramerization and facilitating MAVS interaction (Cadena et al., 2019). Further downstream, MAVS signaling also requires the assembly of a larger prion-like aggregate, which is nucleated by the RIG-I CARD tetramer (Hou et al., 2011; Wu et al., 2014). Although we have clear insights into the activation steps along the RIG-I signaling pathway, the fate of these large signaling complexes remains obscure.

Stress granules are large liquid-like aggregates of RNA and protein that assemble in response to several stimuli (Buchan and Parker, 2009; Ivanov et al., 2018). The assembly of SGs is initiated following the phosphorylation of eIF2a and the activation of its upstream kinases PERK, PKR, GNC2, and HRI. These kinases are part of the integrated stress response (ISR) and activated in response to several stresses (Wek, 2018; Pakos-Zebrucka et al., 2016). PKR binds to viral dsRNA (Srivastava et al. 1998), PERK detects protein mis-folding in the ER (Harding, Zhang, and Ron, 1999), GNC2 senses uncharged tRNAs during nutrient depravation (Dever et al., 1992), and HRI responds to oxidative stress and heme availability (McEwen et al., 2005). Phosphorylated eIF2a inhibits translation by depleting the eIF2•GTP-Met-tRNAi^{Met} tertiary complex, which is required for loading the AUG start codon with Met-tRNAi^{Met} (Kedersha et al., 2002). Shut-down of active translation results in the accumulation of stalled initiation complexes, which serve as the pool of RNA-protein within SGs (Ivanov, Kedersha, and Anderson, 2019). Multiple RNA-binding proteins have been shown to nucleate the condensation of stalled initiation complexes into SGs. The best characterized SG-nucleating proteins are G3BP1 and G3BP2 (Ras-GAP SH3 binding proteins 1 and 2), as well as TIA1 (T-cell Intracellular Antigen 1) and TIAR (TIA-1-related protein) (Kedersha et al., 1999; Kedersha et al., 2002; Kedersha et al., 2016). The assembly of SGs allows cells to rapidly reprogram their translational profile by serving as site of mRNA storage and regulation of their translation (Ivanov, Kedersha, and Anderson, 2019). However, recent work has also shown that SGs play a role in cellular survival or cell-death during different stress conditions or pathological states (Zhang et al., 2019; Reineke et al., 2018; Reineke and Neilson, 2019).

In the context of IFN signaling, SGs are thought to function as antiviral 'hubs,' serving as platforms for the recruitment of signaling molecules and coordinating the signaling events (Onomoto et al., 2013). Multiple signaling molecules, including RIG-I and MDA5, have been shown to co-localize to SGS during viral infection (Onomoto et al., 2013; Oh et al., 2016; Langereis, Feng, and Kuppeveld, 2013). In addition, these SGs contain viral RNA and other antiviral proteins like PKR, RNase L and OASes (Onomoto et al., 2013; Onomoto et al., 2014; Kang et al., 2018). The presence of viral RNA and these antiviral proteins in SGs led to the hypothesis the local concentration of these molecules facilitates signaling. However, previous work on MDA5 (Langereis, Feng, and Kuppeveld, 2013), and our own work in RIG-I (described in chapter 2), suggested that SGs are dispensable for the antiviral response. This raises the questions around the purpose of recruiting RIG-I and other signaling molecules into SGs.

Previous studies have suggested that SGs are cleared through autophagy in the context of chronic stress (Buchan et al., 2013; Reineke and Neilson, 2019; Silva et al., 2019). Here, I provide evidence that RIG-I, along with other signaling molecules, are recruited to SGs and degraded through autophagy in response to dsRNA stimulation. Contrary to the current hypothesis, SGs are not required for RIG-I-mediated anti-viral signaling, but rather suppress signaling by sequestering and degrading signaling complexes. Finally, the lack of a clearing mechanism in the absence of SGs led to a caspase-dependent cell death that requires the RIG-I-like receptor and MAVS signaling, but was independent of their IFN inducing activities. Although this work remains in progress, I propose that SGs play a critical role in suppressing aberrant IFN signaling and a live-or-die cell fate decision in response to dsRNA-mediated stress.

3.3 Methods

3.3.1 Cell lines

U2OS cell lines were used for all experiments in this work. The parental wild-type U2-OS and G3BP1 and G3BP2 double knock-out cell lines were kindly provided by Dr. Paul J. Anderson and described elsewhere (Kedersha et al., 2016). U2OS cell lines stably expression GFP-RIG-I, GFP-MAVS, and GFP-RIPLET (pcDNA3.1) were established using transient transfection, then selection with 0.5mg/mL Neomycin (G418). Single clones were selected using limiting dilution and screened using fluoresce microscopy and western blotting. MAVS, RNase L, and IRF3 were knocked-out in G3BP1/2 KO U2-OS using the pLentiCRISPRv2 vector and lentiviral transduction. The gRNAs were: MAVS (for: CACCG CCAGCCGGGCCGCCGCTGAA, rev: AAAC TTCAGCGGCGGCCCGGCTGG C); RNase L (for: CACCG TTTGAGGCGAAAGACAAAGG, rev: AAAC CCTTTGTCTTTCGCCTCAAAC); IRF3 (for: CACCG GACACCTCTCCGGACACCAA, rev: AAAC TTGGTGTCCGGAGAGGTGTC C). Following transduction, cells were selected with 1ug/mL puromycin for one week and knock-out confirmed by immunoblotting and genomic PCR. The All cells were maintained at 5.0% CO2 in DMEM containing 10% FBS and 1% L-glutamine.

3.3.2 Synthesized RNA

Double-stranded RNAs (dsRNAs) were prepared by in vitro T7 transcription as previously described (Peisley et al., 2011). The sequences of the 162 dsRNAs were taken from the first 150 bp of the MDA5 gene flanked by 5'-gggaga and 5'-tctccc. The 162bp dsRNAs contains a 5'ppp and blunt end. The two complementary strands were co-transcribed, and the duplex was separated from unannealed ssRNAs by 8.5% acrylamide (28-162 bp) gel electrophoresis in TBE

buffer. RNA was gel-extracted using the Elutrap electroelution kit (Whatman), ethanol precipitated, and stored in 20 mM Hepes, pH 7.0. Qualities of RNAs were analyzed by 1X TBE polyacrylamide gel.

3.3.3 Antibodies

For immuno-blotting, antibodies and their manufacturers were: Rabbit α-RIG-I (ENZO), rabbit α-β-actin (Cells Signaling), rabbit α-IRF3 (Cell Signaling), rabbit α-Phospho-IRF3 (Cell Signaling), rabbit α-caspase 3 (Cell Signaling), rabbit α-caspase 9 (Cell Signaling), and mouse α-caspase 8 (Cell Signaling). For immunofluorescence, antibodies included: α-RIG-I (in-house) (Oh et al., 2016) and α-TIAR (Santa Cruz), G3BP1 (Santa Cruz), α-MAVS (Bethyl Laboratories).

3.3.4 Immunoblotting

All experiments were done in a 6-well format (~500 000/well seeded). Cells were transfected with 1ug of 162bp dsRNA and harvested 6 hours or 24 hours post-transfection. Cells were harvested by scrapping, then pelleted by spinning down at 16000g for 20 seconds. The cell pellet was washed with 200uL PBS, then spin down again. The cell pellet was lysed with 50uL of 1% SDS lysis buffer (10mM Tris 7.5, 150mM NaCl, 10mM DTT, 1% SDS), then boiled for 10min. Proteins were resolved on 4–15% gradient gels (Invitrogen), transferred to PVDF membranes, and blotted using standard procedures.

3.3.5 RT-qPCR

All experiments were done in a 24-well format (~100000 cells/well seeded). Cells were transfected with 200ng of 162bp dsRNA and harvested at 6 hours or 24 hours post-transfection.

Total RNAs were extracted using TRIzol reagent (Thermo Fisher) and cDNA was synthesized using High Capacity cDNA reverse transcription kit (Applied Biosystems) according to the manufacture's instruction. Real-time PCR was performed using a set of gene specific primers (see the Table S1), a SYBR Green Master Mix (Applied Biosystems), and the StepOne™ Real-Time PCR Systems (Applied Biosystems).

3.3.6 Immunofluorescence imaging

Cells were stimulated with 500ng of 162 bp dsRNA for 6 hours. Cells were fixed with 2% paraformaldehyde at RT for 10 minutes, and permeabilized with 0.5% Triton-X at RT for 10 minutes. Cells were blocked for 30 min at RT with 1% BSA in PBST and stained using primary antibodies overnight. Images were obtained using a Zeiss Axio Imager M1 microscope at 100X magnification.

3.3.7 Flow Cytometry

All experiments were done in 12-well format (~200000 cells/well). 20 minutes prior to dsRNA transfection, the media was changed and contained 10 μM pan-caspase inhibitor (Q-VD-OPh, Santa Cruz) or DMSO. Cells were transfected with 500ng of 162bp dsRNA for 24 hours, collected using trypsin, and washed with PBS. The cells were stained with 2uM Sytox (Thermo) in FACS buffer (1% FBS, 25mM Tris pH 7.5, 1mM EDTA in PBS) for 15 minutes. Cells were analyzed using a FACS Canto II flow cytometer and BD FACS Diva software.

3.4 Results

3.4.1 The RIG-I signaling complex is recruited to SGs and degraded through autophagy

We, along with other groups, have shown that endogenous RIG-I forms granules in the presence of dsRNA (Cadena et al. 2019) or viral infection (Oh et al. 2016) using Immunofluorescence (IF). These granules co-localize with G3BP1 and TIA, known markers of SGs (Figure 3.1A and 3.1D). Next, we wanted to know if other components of the IFN signaling pathway also co-localize with SGs. The ubiquitin ligase RIPLET, which is critical for the signaling activity of RIG-I, also formed granules that co-localized with SGs (Figure 3.1B). Further downstream, the adaptor protein MAVS (Figure 3.1C), as well as the signaling molecules TRAF3 and TRAF5 (Figure S6A). G3BP1 and G3BP2 are known nucleators of SGs. To test if the RIG-I granule formation precedes SG formation, we knocked-out G3BP1 and G3BP2 from cells (from here on referred to as G3BP1/2 KO). RIG-I did not form granules in the cells lacking these genes (Figure 3.1D), suggesting that the observed granules are *bona fide* SGs. Our previous work demonstrated that treatment of cells with cycloheximide (CHX), which is known to prevent SG formation (chapter 2), did not negatively impact IFN signaling in response to dsRNA stimulation (also explored further below), raising the question of why IFN signaling complexes are recruited to SGs. Previous reports have suggested that autophagy contributes to the clearance of SGs under conditions of chronic stress (Buchan et al., 2013; Reineke and Neilson, 2018). We hypothesized that dsRNA mediated SGs are a conduit for the degradation of IFN signaling complexes during signaling. Consistent with this idea, dsRNA stimulation induced the formation of granules containing LC3, a known marker of autophagy, that co-localized with RIG-I (Figure 3.1E). The co-localization of RIG-I and LC3 was completely abolished in the G3BP1/2 KO cells

(Figure 3.1E). These results suggest that the recruitment of signaling aggregates to SGs after dsRNA stimulation is a mechanism for their degradation by autophagy.

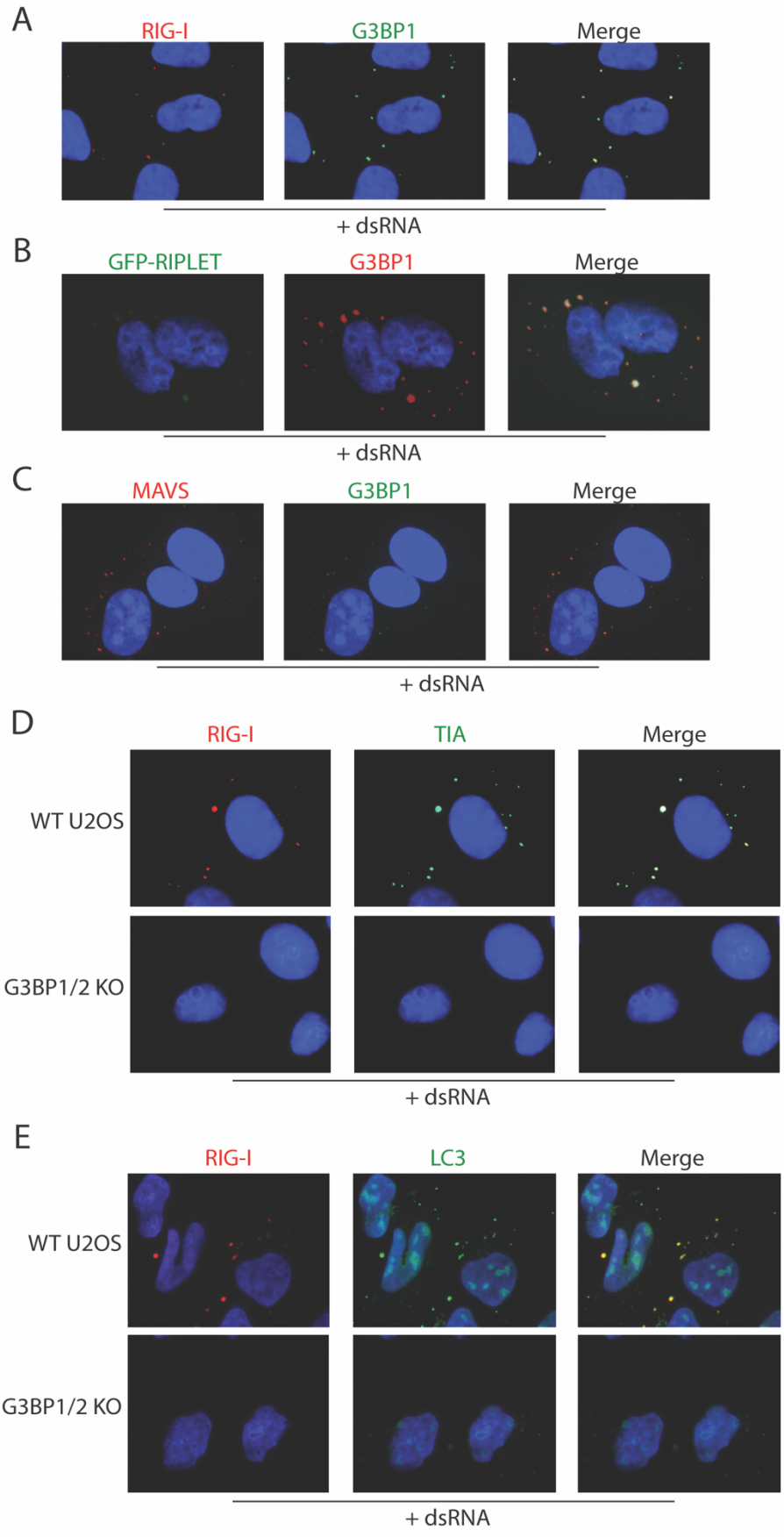

A
RIG-I
G3BP1
Merge
+ dsRNA
B
GFP-RIPLET
G3BP1
Merge
+ dsRNA
C
MAVS
G3BP1
Merge
+ dsRNA
D
RIG-I
TIA
Merge
WT U2OS
G3BP1/2 KO
+ dsRNA
E
RIG-I
LC3
Merge
WT U2OS
G3BP1/2 KO
+ dsRNA

Figure 3.1 RIG-I Signaling complexes are recruited to SGs

3.1A) Representative immunofluoresce images of endogenous RIG-I and endogenous G3BP1 in the presence of 162bp dsRNA (0.5µg). Cells were fixed 6 hours post-stimulation. **3.1B)** Representative immunofluoresce images of GFP-RPLET and endogenous G3BP1 in the presence of 162bp dsRNA (0.5µg). Cells were fixed 6 hours post-stimulation. Of note, antibodies for the detection of endogenous RIPLET by IF are not available. These images were taken in cells stably expressing GFP-RIPLET (see methods). **3.1C)** Representative immunofluoresce images of endogenous MAVS and endogenous G3BP1 in the presence of 162bp dsRNA (0.5µg). Cells were fixed 6 hours post-stimulation. **3.1D)** Representative immunofluoresce images of endogenous RIG-I and endogenous TIA in the presence of 162bp dsRNA (0.5µg) in wild-type (WT) and G3BP1/2 KO U2OS. Cells were fixed 6 hours post-stimulation. **3.1E)** Representative immunofluoresce images of endogenous RIG-I and endogenous LC3 in the presence of 162bp dsRNA (0.5µg) in wild-type (WT) and G3BP1/2 KO U2OS. Cells were fixed 6 hours post-stimulation.

3.4.2 SGs suppress RIG-I Signaling

SGs have been suggested to act as 'hubs' for orchestrating signaling events (Onomoto et al., 2013). This hypothesis is based on the recruitment of RIG-I and other antiviral proteins to SGs. Furthermore, knock-down of the SG-nucleating protein G3BP1 led to a deficiency in antiviral signaling (Onomoto et al., 2013). If SGs are involved in the degradation of RIG-I signaling complexes, then we expect to see an increase in signaling. To test this hypothesis, we stimulated WT and G3BP1/2 KO cells with a RIG-I-specific ligand (162bp dsRNA, see chapter 2). Using this model ligand is also beneficial given that viral infection can have confounding indirect effects in signaling and SG assembly. We stimulated cells for 6 or 24 hours, then measured the expression IFN-β mRNA, as well as other antiviral genes (Figure 3.2A). Consistent with the lack of degradation of the signaling complexes, the G3BP1/2 KO cells showed increased expression of these genes at 6hrs. In addition to mRNA expression, we monitored upstream IFN signaling events, like the phosphorylation of the transcription factor IRF3. Consistent with the mRNA results, the G3BP1/2 showed higher phosphorylation IRF3 at 6 hours (Figure 3.2B). Of note, the expression of IFN-β mRNA in G3BP1/2 KO cells decreased at 24 hours, resulting in two-fold lower reduction compared to wild-type cells. This is consistent with deficiency in RIG-I antiviral signaling in previous studies (Onomoto et al., 2013). We will explore this drop in the IFN signaling at 24 hours in the paragraphs below. However, the higher activation at earlier time-points is consistent with a role for SGs in suppressing signaling rather than their requirement as orchestrating hubs. If the higher signaling in G3BP1/2 KO cells is the result of a lack of degradation of the signaling complexes, then knock-out of genes involved in autophagy produce a similar effect. We performed a similar experiment in ATG7 knock-out cells, which are

known to be deficient in the autophagy pathway (Figure 3.2C). Like the G3BP1/2 KO cells, knock-out of ATG7 also led to higher IFN-β mRNA expression and phosphorylation of IRF3. Of note, the effect occurred at a later time-point in the ATG7 KO cells than G3BP1/2 KO. This is likely because these cells can still form SGs, and thus sequester IFN signaling complexes, preventing higher activation at earlier time-points.

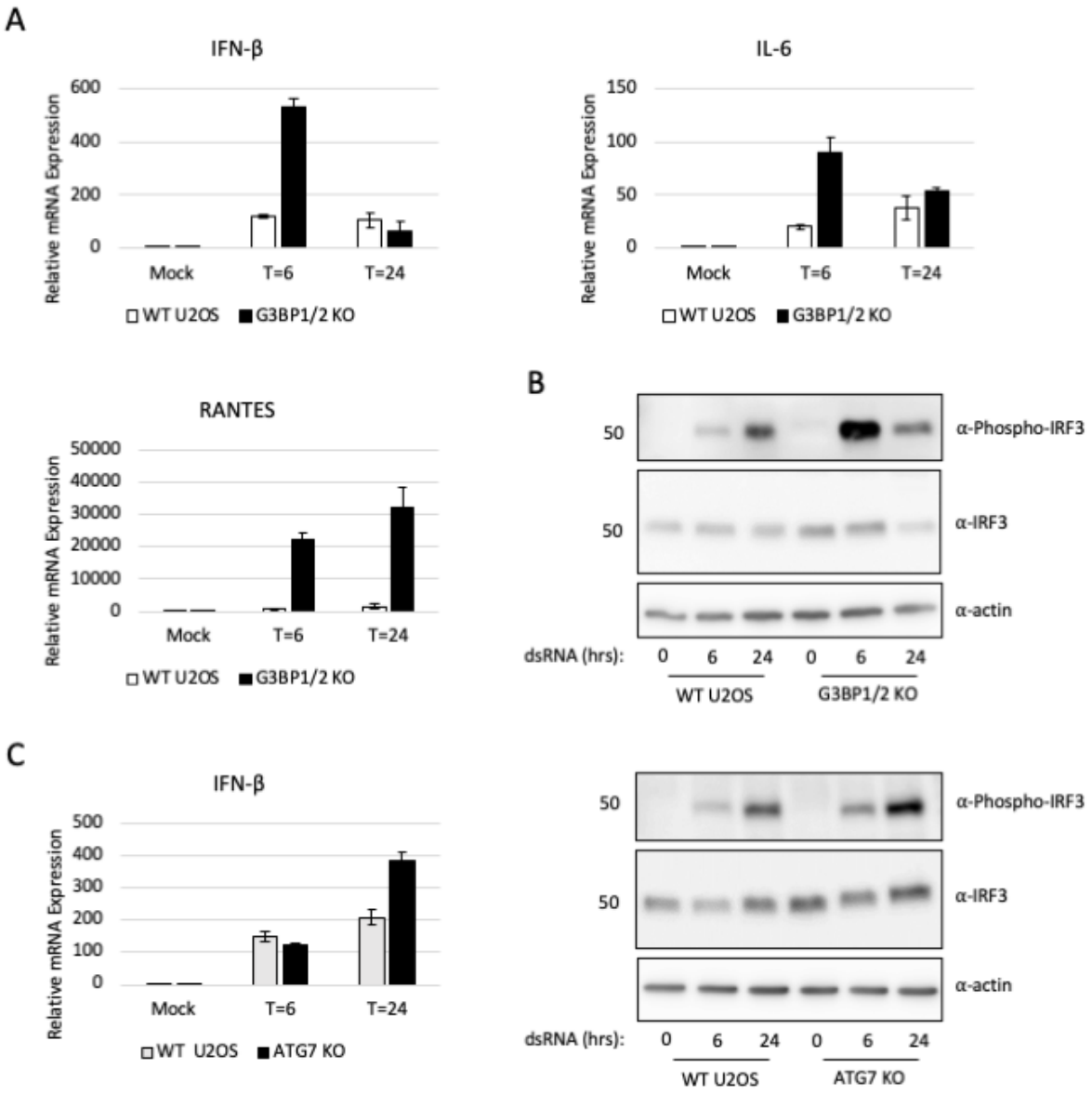

A
IFN-β
Relative mRNA Expression
600
400
200
0
Mock
T=6
T=24
WT U2OS
G3BP1/2 KO
IL-6
150
100
50
0
RANTES
50000
40000
30000
20000
10000
B
α-Phospho-IRF3
α-IRF3
α-actin
50
dsRNA (hrs):
0
6
24
WT U2OS
G3BP1/2 KO
C
500
400
300
200
100
ATG7 KO

Figure 3.2 SGs suppress RIG-I signaling

3.2A) Relative level of antiviral signaling in U2OS cells (WT and G3BP1/2 KO), as measured by the level of IFN-β, IL-6, and RANTES mRNAs by qPCR. All data are presented as mean ± s.d. (n = 3-4) and are representative of at least three independent experiments. 3.2B) Representative immunoblot for the phosphorylation of IRF3 in U2OS (WT and G3BP1/2 KO) at 6- and 24-hours post dsRNA stimulation. 3.2C) Relative level of antiviral signaling in U2OS cells (WT and ATG7 KO), as measured by the level of IFN-β mRNA (left) and phosphorylated IRF3 (right).

3.4.3 SGs are critical for cell survival after dsRNA stimulation

In our attempt to examine the IFN signaling in G3BP1/2 KO in late time-points, we noticed that these cells were more sensitive to dsRNA-mediated cell-death than the wild-type (Figure 3.3A-B). G3BP1/2 KO cells showed more increased caspase 3 cleavage (Figure 3.3C) and their cell death was rescued fully by the addition of the pan-caspase inhibitor Q-VD-OPh (Figure 3.3B). This suggests that the mechanism of cell death in these cells is apoptosis. Next, we wanted to examine which type of apoptotic cell death is initiated in the G3BP1/2 KO cells. Immunoblotting for active caspase 8 (involved in extrinsic apoptosis) and caspase 9 (involved in the intrinsic apoptosis) showed that these cells engage in both pathways (Figure 3.3C), suggesting a possible interaction between these pathways (McComb et al., 2019).

Cell-death in response to dsRNA stimulation has been studied in the context of RNase L activation (Castelli et al., 1998; Li et al., 2017). RNase L is a nuclease that cleaves viral and cellular RNAs during infection. RNase L is activated by OASes (2'-5'-oligoadenylate synthetases), which are upregulated during the IFN response. We explored whether the death in G3BP1/2 KO cells is mediated by RNase L by deleting RNase L or MAVS in our G3BP1/2 KO cells. Knock-out of RNase L partially rescued cell-death in G3BP1/2 (Figure 3.3D). Interestingly, knock-out of MAVS had a pronounced effect in the death of G3BP1/2 KO cells, independent of the activity of RNase L (Figure 3.3D). This suggests that MAVS plays a role in ameliorating cell death in the absence of SGs independent of IFN signaling. Consistent with this idea, knock-out of IRF3 in G3BP1/2 KO cells did not rescue cell death (Figure S7A).

Previously, we observed a robust decrease in the expression of IFN-β mRNA and the phosphorylation of IRF3 at 24 hours post dsRNA stimulation. This decrease is concomitant with cell death in G3BP1/2 KO cells. These results raise the possibility that cell death is responsible for the decrease in IFN signaling at this time-point. To test this, we examined the expression of IFN-β mRNA at 24 hours in the presence of the pan-caspase inhibitor, which fully rescues cell death (Figure 3.3A-B). Expression of IFN-β mRNA was robustly increased in the presence of the pan-caspase inhibitor at 24 hours (Figure 3.3E). Importantly, the pan-caspase inhibitor did not affect the expression of IFN-β mRNA at the early time-point, when cells do not yet show apparent cell death. Of note, the pan-caspase inhibitor also has an effect on the signaling of WT cells at 24 hours. Although the cell death in WT cells is not pronounced (Figure 3.3A-B), these cells do show cleavage of caspases at this time-point (Figure 3.3C), suggesting that engagement of the cell death pathway alone is sufficient to negatively affect IFN signaling.

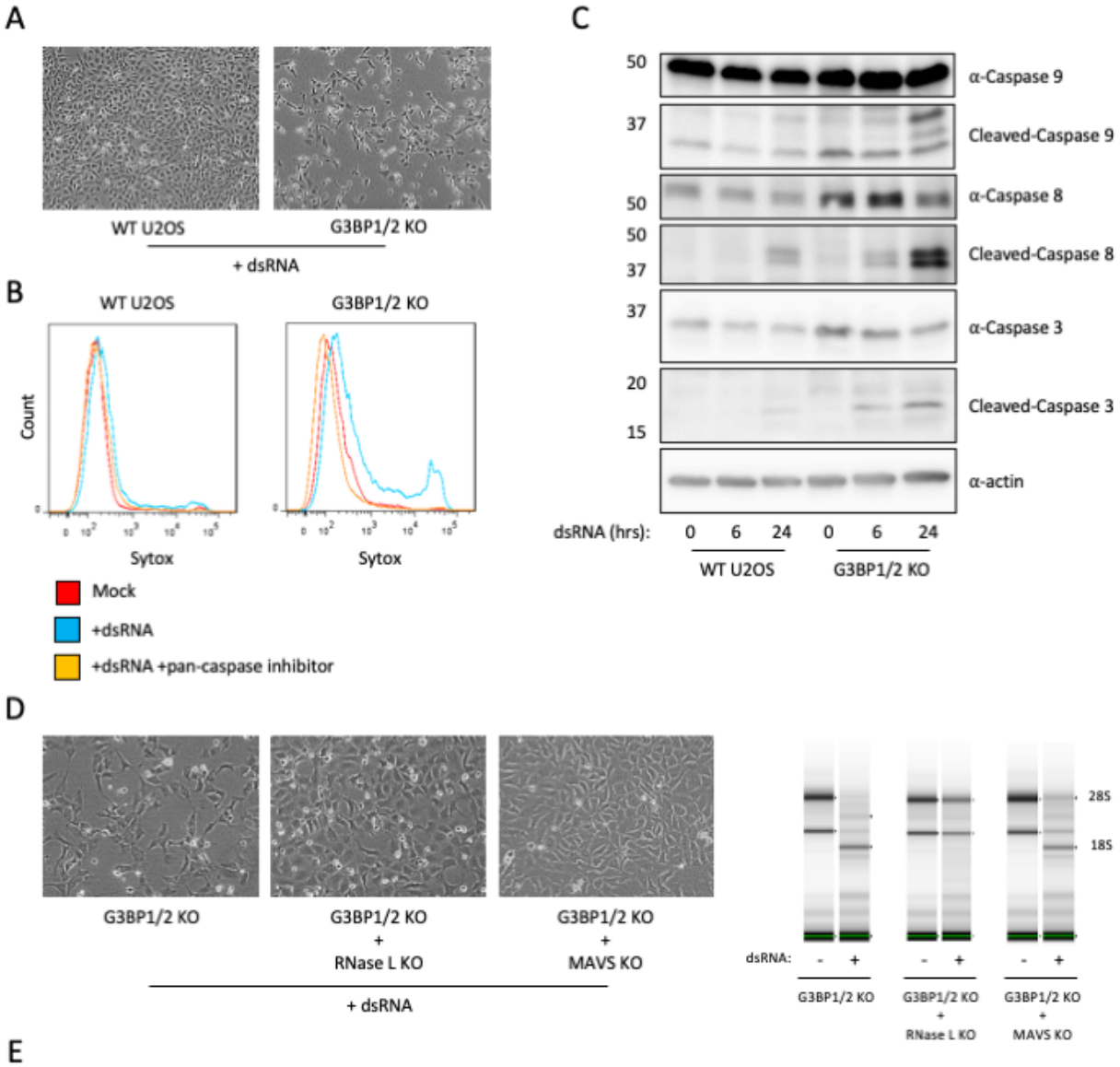

A
WT U2OS
G3BP1/2 KO
+ dsRNA
B
WT U2OS
G3BP1/2 KO
Count
Sytox
Sytox
Mock
+dsRNA
+dsRNA +pan-caspase inhibitor
C
50
α-Caspase 9
37
Cleaved-Caspase 9
50
α-Caspase 8
50
37
Cleaved-Caspase 8
37
α-Caspase 3
20
15
Cleaved-Caspase 3
α-actin
dsRNA (hrs): 0 6 24 0 6 24
WT U2OS
G3BP1/2 KO
D
G3BP1/2 KO
G3BP1/2 KO + RNase L KO
G3BP1/2 KO + MAVS KO
+ dsRNA
28S
18S
dsRNA: - + - + - +
G3BP1/2 KO
G3BP1/2 KO + RNase L KO
G3BP1/2 KO + MAVS KO
E
Relative IFN-β mRNA Expression
1800
1600
1400
1200
1000
800
600
400
200
0
Mock T=6 T=24 Mock T=6 T=24 Mock T=6 T=24 Mock T=6 T=24
WT U2OS
G3BP1/2 KO
WT U2OS
G3BP1/2 KO
DMSO
Pan-Caspi

Figure 3.3 SGs are critical for cell survival after dsRNA stimulation

3.3A) Representative light microscopy images of U2OS (WT and G3BP1/2 KO) stimulated with 162bp dsRNA (1µg) for 24 hours. 3.3B) Sytox staining of U2OS (WT and G3BP1/2 KO) stimulated with 162bp dsRNA (1µg) for 24 hours in the presence of the pan-caspase inhibitor Q-VD-OPh. The incorporation of sytox (death cells) was measure using flow cytometry. 3.3C) Representative immunoblot for the cleavage of caspases in U2OS (WT and G3BP1/2 KO) at 6- or 24-hours post dsRNA stimulation (1ug). 3.3D) Representative light microscopy images of U2OS (G3BP1/2 KO, G3BP1/2 RNase L KO, and G3BP1/2 MAVS KO) stimulated with 162bp dsRNA (1µg) for 24 hours (left). Total RNA from each cell line was analyzed by electrophoresis a using an Agilent TapeStation system to confirm the activity of RNase L (right). Relative level of antiviral signaling in U2OS cells (WT and G3BP1/2 KO) in the presence of the pan-caspase inhibitor, as measured by the level of IFN-β mRNA. All data are presented as mean ± s.d. (n = 3-4) and are representative of at least three independent experiments.

3.5 Discussion

We have provided evidence that stress granules play a key role in suppressing aberrant IFN signaling (Figure 3.2). Knock-out of the SG-nucleating proteins G3BP1 and G3BP2 led to higher expression of IFN-β and other antiviral genes, as well as higher phosphorylation of the transcription factor IRF3 during the early steps of signaling. These results contrast the current hypothesis that SGs orchestrate signaling events, and thus are required for signaling to occur (Onomoto et al., 2013; Onomoto et al., 2014). This prevailing hypothesis is based partly on the IFN signaling deficiency of G3BP1/2 knocked-down cells at late stages in the antiviral response. We also observed a similar phenotype in our knock-out cell lines at 24hrs (Figure 3.2). However, we demonstrate that the decrease in IFN signaling in G3BP1/2 KO cells from 6- to 24-hours is due to a cell death process. Preventing cell death using the pan-caspase inhibitor reversed this 'drop' in IFN signaling, suggesting an interplay between cell death and IFN signaling.

Rather than serving as 'hubs' for orchestrating signaling events, we propose that SGs are intermediates in the degradation of IFN signaling complexes. We showed that not only RIG-I, but also other signaling molecules, including RIPLET, MAVS, and TRAF2/6, are recruited to SGs. Importantly, the co-localization of RIG-I with LC3, an autophagy marker, depended on the assembly of SGs (Figure 3.1), which suggests a possible degradation mechanism. Our work in this front is not finished and we are currently testing the autophagic flux of these proteins. However, the lack of sequestration of these signaling complexes into SGs in G3BP1/2 KO U2OS, and the lack of subsequent degradation by autophagy, is consistent with the hyper-activation of IFN signaling we observed (figure 3.2).

Finally, we showed that SGs are critical determinants of cell death in response to dsRNA stimulation. G3BP1/2 KO cells were more sensitive to dsRNA than the WT parental cells at 24 hours, and this cell death was fully ameliorated with pan-caspase inhibitor treatment. We also observed more cleavage of the effector caspase 3 in G3BP1/2 KO cells, which suggests that their cell death was due to apoptosis. Our current work is trying to mechanistically determine the steps leading to apoptotic cell death in these cells. While this work continues, our results thus far suggest that SGs are critical in preventing hyperinflammation in response to dsRNA and are check-points in a life-death decision in cells.

Chapter 4: Conclusion

4.1 Binding of Ubiquitin ligases to RLRs

Here we described the mechanistic details of the binding between the ubiquitin ligase RIPLET and its substrate RIG-I. We discovered that the binding between RIPLET and RIG-I requires bivalent RIPLET PRY/SPRY domains and that at least two RIG-I molecules need to be present in the RIG-I filament. This work provides the foundation for future efforts in the structural understanding of the RIPLET-RIG-I interaction, as well as the interaction between RIG-I-like receptors and other ubiquitin ligases.

Although further detailed structural work is still missing, the model presented in chapter two for the interaction between RIG-I and RIPLET is an important first step. Given that RIG-I filaments form a heterogenous population, and that the addition of RIPLET causes the aggregation of these filaments, the study of the RIPLET-RIG-I complex using full-length proteins would be difficult using cryo-electron microscopy (due to lack of heterogeneity of the sample) or crystallography (because large and flexible molecular complexes are difficult to crystallize). Instead, future structural work should focus on the minimal interaction domain that we described here. First, we discovered that RIPLET binds to the helicase-CTD of RIG-I, and thus we could omit the N-terminal 2CARD domain along with the flexible linker between the 2CARD and the helicase domain (~200 residues total). Further truncation of the helicase domain and the CTD inhibited RIPLET binding (not shown in chapter 2), thus this unit is minimally required.

Second, we discovered that a 21bp dsRNA is minimally required to allow for RIPLET-RIG-I interaction. The dsRNA footprint of RIG-I is 10-12bp long, thus any dsRNA shorter than 21bp would lack the minimal two RIG-I molecules required for RIPLET binding. In addition, any dsRNA

beyond 30-40bp would allow multiple binding confirmations between RIG-I and RIPLET, increasing the heterogeneity of the sample. Lastly, rather than using full-length RIPLET or the RING-deletion mutant, future studies should focus on using our GST-PRY/SPRY construct. The benefit of using GST-PRY/SPRY is that, although this protein binds RIG-I filaments more efficiently than the RIPLET RING-deletion mutant, it does not induce clustering, thus reducing the heterogeneity of the sample. The predicted molecular weight of this minimal RIG-I complex is ~ 200 kd, which falls above the minimal ~100 kd suitable for electron microscopy.

In addition to RIG-I, cells can also sense cytoplasmic viral dsRNA through the receptor MDA5. Both RIG-I and MDA5 belong to the RLR family and comprise similar domain architecture (2CARD-helicase-CTD) and share the same downstream pathway (MAVS). Like RIG-I, the 2CARD domain of MDA5 was also shown to be ubiquitinated, and this modification was shown to promote signaling. However, the identity of the ubiquitin ligase involved in MDA5 ubiquitination remained a mystery. Recently, TRIM65 was discovered as the ubiquitin ligase involved in MDA5 signaling (Lang et al., 2016). Like RIPLET, TRIM65 contains a C-terminal PRY/SPRY domain and a central coiled-coil domain. Given their domain similarity, it will be interesting to test if the interaction between MDA5 filaments and TRIM65 parallels that of RIPLET and RIG-I. For example, we can purify the PRY/SPRY domain of TRIM65 tagged with GST to test the bivalency requirement. Since the TRIM65 coil-coiled domain is likely to be in antiparallel symmetry, we can also test if TRIM65 is able to cluster MDA5 filaments, and whether or not clustering can promote signaling in the absence of ubiquitination using a RING-deletion mutant.

Our discovery of the bivalency requirement for the interaction between RIPLET and RIG-I shows how ubiquitin ligases can discriminate their substrates based on their oligomerization state. It would be intriguing to test if the bivalency requirement can be applied to other ubiquitin ligases that are important for antiviral signaling, not only during the activation of the receptors but also after signaling. For example, RNF125 has been shown to negatively regulate RIG-I signaling (Arimoto et al., 2007). Unlike RIPLET, which conjugates activating K63-linked Ub chains, RNF125 conjugates K48-linked ubiquitin. This type of ubiquitination leads to the degradation of RIG-I, thus preventing its aberrant signaling. The direct interaction between RNF125 and RIG-I has not been studied, but it is intriguing to think that this ligase could also recognize pre-oligomerized RIG-I using a similar binding mode as RIPLET. Our work on RIPLET opened new hypotheses to study the interaction between receptors and ligases in antiviral innate immunity.

4.2 Identification of factors involved in SG resolution

Here we showed that the critical RLR signaling adaptor MAVS co-localizes with LC3, an autophagy marker, after dsRNA stimulation. This co-localization was completely abolished in cells lacking G3BP1/2, which are the nucleators of dsRNA-mediated SGs, and this led to the hyper-activation of the IFN signaling pathway in response to dsRNA. This suggest that SGs are important for the degradation of MAVS signaling complexes through autophagy.

To test this hypothesis further, we are currently developing a system to express MAVS tagged with keima in stable cells. Keima is a florescent protein that undergoes a change in its excitation/emission depending on the pH. Keima is excited at a 448 nm under neutral pH, but

this changes in an acidic pH, where the excitation changes to 580 nm. This approach has been used previously to the test the flux of proteins into the lysosome (An et al., 2019). The change in the excitation/emission of keima-MAVS in response to dsRNA could indicate its flux into the lysosome. In addition to providing further evidence for the flux of MAVS into the lysosome, this system could be useful for the identification of factors involved in the degradation of SGs through autophagy in a genome-wide knock-out screen. Cells that have deletions in factors involved in the flux of keima-MAVS into the lysosome will fail to undergo a keima excitation/emission shift and can be sorted using FACS. To our knowledge, this could be the first screen use to identify factors that mediate the resolution of signaling aggregates in an innate signaling pathway. Our work on SGs and their relationship to RLR signaling lay the groundwork for these future efforts.

4.3 Understanding the RIG-I signaling pathway from beginning to end

Our work in this dissertation has uncovered important steps in the activation and shut-down of the RIG-I signaling pathway. We challenged the long-standing dogma in the field that TRIM25 is the required ubiquitin ligase for RIG-I and showed that RIPLET is solely needed. In addition, we discovered that this ubiquitin ligase has functions other than ubiquitination in promoting antiviral signaling by assembling RIG-I aggregates. In our efforts to further understand these RIG-I and MAVS signaling aggregates, we discovered the reason for their recruitment into stress granules. Rather than promoting the signaling of RIG-I and MAVS, as is the current hypothesis in the field, we discovered that SGs suppress RIG-I signaling. This suppression of signaling is due to the sequestration of these signaling molecules and leads to their degradation through autophagy. Although much more work is needed to fully understand

RIG-I signaling, our work provided insight into the early steps of RIG-I activation, the recruitment of RIG-I and MAVS into SGs, and the subsequent degradation of the signaling aggregates through autophagy.

Appendix 1: References

Ahmad, S., Mu, X., Yang, F., Greenwald, E., Park, J.W., Jacob, E., Zhang, C.Z., and Hur, S. (2018). Breaching self-tolerance to Alu duplex RNA underlies MDA5-mediated inflammation. *Cell* 172, 797-810.

Alexandrov, A., Dutta, K., and Pascal, S.M. (2001). MBP Fusion Protein with a Viral Protease Cleavage Site: One-Step Cleavage/Purification of Insoluble Proteins. BioTechniques 30, 1194-1198.

An H., Ordureau A., Paulo J.A., Shoemaker C.J., Denic V., and Harper J.W. (2019). TEX264 Is an Endoplasmic Reticulum-Resident ATG8-Interacting Protein Critical for ER Remodeling during Nutrient Stress. Mol Cell 74: 891—908.

Andreeva, L., Hiller, B., Kostrewa, D., Lassig, C., de Oliveira Mann, C.C., Jan Drexler, D., Maiser, A., Gaidt, M., Leonhardt, H., Hornung, V., et al. (2017). cGAS senses long and HMGB/TFAM-bound U-turn DNA by forming protein-DNA ladders. Nature 549, 394-398.

Antos, J.M., Chew, G.-L., Guimaraes, C.P., Yoder, N.C., Grotenbreg, G.M., Popp, M.W.-L., and Ploegh, H.L. (2009). Site-specific N- and C-terminal labeling of a single polypeptide using sortase of different specificity. J Am Chem Soc 131, 10800-10801.

Arimoto, K., Takahashi, H., Hishiki, T., Konishi, H., Fujita, T., and Shimotohno, K. (2007) Negative regulation of the RIG-I signaling by the ubiquitin ligase RNF125. PNAS 104: 7500—7505.

Binder, M., Eberle, F., Seitz, S., Mucke, N., Huber, C.M., NKiani, N., Kanderali, L., Lohmann, V., Dalpke, A., and Bartenschlager, R. (2011). Molecular mechanism of signal perception and integration by the innate immune sensor retinoic acid inducible gene-I. J Biol Chem 286, 27278-27287.

Buchan, J. R., Kolaitis, R. M., Taylor, J. P., and Parker, R. (2013). Eukaryotic stress granules are

cleared by autophagy and Cdc48/VCP function. Cell, 153(7), 1461-1474.

Buchan, J. R., & Parker, R. (2009). Eukaryotic stress granules: the ins and outs of translation. Molecular cell, 36(6), 932-941.

Cadena, C., Ahmad, S., Xavier, A., Willemsen, J., Park, S., Park, J.W., Oh, S.W., Fujita, T., Hou, F., Binder, M., *et al.* (2019). Ubiquitin-dependent and-independent roles of E3 ligase RIPLET in innate immunity. Cell, 177(5), 1187-1200.

Cadena, C., & Hur, S. (2019). Filament-like Assemblies of Intracellular Nucleic Acid Sensors: Commonalities and Differences. Molecular Cell, 76(2), 243-254.

Castelli, J.C., Hassel, B.A., Maran, A., Paranjape, J., Hewitt, J.A., Li, X.L., Hsu, Y.T., Silverman, R.H., and Youle, R.J. (1998). The role of 2′-5′ oligoadenylate-activated ribonuclease L in apoptosis. Cell Death & Differentiation, 5(4), 313-320.

Choudhury, N.R., Heikel, G., Trubitsyna, M., Kubik, P., Nowak, J.S., Webb, S., Granneman, S., Spanos, C., Rappsilber, J., Castello, A., et al. (2017). RNA-binding activity of TRIM25 is mediated by its PRY/SPRY domain and is required for ubiquitination. BMC Biol 15, 105.

Choudhury, N.R., Nowak, J.S., Zuo, J., Rappsilber, J., Spoel, S.H., and Michlewski, G. (2014). Trim25 Is an RNA-Specific Activator of Lin28a/TuT4-Mediated Uridylation. Cell Rep 9, 1265-1272.

Devarkar, S.C., Schweibenz, B., Wang, C., Marcotrigiano, J., and Patel, S.S. (2018). RIG-I Uses an ATPase-Powered Translocation-Throttling Mechanism for Kinetic Proofreading of RNAs and Oligomerization. Mol Cell 72, 355-368 e354.

Dever, T. E., Feng, L., Wek, R. C., Cigan, A. M., Donahue, T. F., & Hinnebusch, A. G. (1992).

Phosphorylation of initiation factor 2α by protein kinase GCN2 mediates gene-specific translational control of GCN4 in yeast. Cell, 68(3), 585-596.

Dong, K.C., Helgason, E., Yu, C., Phu, L., Arnott, D.P., Bosanac, I., Compaan, D.M., Huang, O.W., Fedorova, A.V., Kirkpatrick, D.S., et al. (2011). Preparation of distinct ubiquitin chain reagents of high purity and yield. Structure 19, 1053-1063.

Gack, M.U., Shin, Y.C., Joo, C.H., Urano, T., Liang, C., Sun, L., Takeuchi, O., Akira, S., Chen, Z., Inoue, S., et al. (2007). TRIM25 RING-finger E3 ubiquitin ligase is essential for RIG-I-mediated antiviral activity. Nature 446, 916-920.

Gao, D., Yang, Y.K., Wang, R.P., Zhou, X., Diao, F.C., Li, M.D., Zhai, Z.H., Jiang, Z.F., and Chen, D.Y. (2009). REUL is a novel E3 ubiquitin ligase and stimulator of retinoic-acid-inducible gene-I. PLoS One 4, e5760.

Goubau, D., Schlee, M., Deddouche, S., Pruijssers, A.J., Zillinger, T., Goldeck, M., Schuberth, C., Van der Veen, A.G., Fujimura, T., Rehwinkel, J., et al. (2014). Antiviral immunity via RIG-I-mediated recognition of RNA bearing 5'-diphosphates. Nature 514, 372-375.

Harding, H. P., Zhang, Y., and Ron, D. (1999). Protein translation and folding are coupled by an endoplasmic-reticulum-resident kinase. Nature, 397(6716), 271-274.

Hartman, N.C., and Groves, J.T. (2011). Signaling clusters in the cell membranes. Curr Opin Cell Biol 23, 370-376.

Hornung, V., Ellegast, J., Kim, S., Brzózka, K., Jung, A., Kato, H., Poeck, H., Akira, S., Conzelmann, K.K., Schlee, M*., et al.* (2006). 5'-Triphosphate RNA is the ligand for RIG-I. Science 314, 994-997.

Hou, F., Sun, L., Zheng, H., Skaug, B., XJiang, Q.X., and Chen, Z.J. (2011). MAVS forms functional prion-like aggregates to activate and propagate antiviral innate immune response. Cell 146, 1-14.

Ivanov, P., Kedersha, N., and Anderson, P. (2019). Stress granule and processing bodies in translational control. Cold Spring Harb Perspect Biol. 11(5).

Jiang, F., Ramanathan, A., Miller, M.T., Tang, G.-Q., Gale, M., Jr., Patel, S.S., and Marcotrigiano, J. (2011). Structural basis of RNA recognition and activation by innate immune receptor RIG-I. Nature 479, 423-427.

Jiang, X., Kinch, L.N., Brautigam, C.A., Chen, X., Du, F., Grishin, N.V., and Chen, Z.J. (2012). Ubiquitin-Induced Oligomerization of the RNA Sensors RIG-I and MDA5 Activates Antiviral Innate Immune Response. Immunity 36, 959-973.

Kang, J. S., Hwang, Y. S., Kim, L. K., Lee, S., Lee, W. B., Kim-Ha, J., & Kim, Y. J. (2018). OASL1 traps viral RNAs in stress granules to promote antiviral responses. Molecules and cells, 41(3), 214.

Kato, H., Takeuchi, O., Sato, S., Yoneyama, M., Yamamoto, M., Matsui, K., Uematsu, S., Jung, A., Kawai, T., Ishii, K.J.*, et al.* (2006). Differential roles of MDA5 and RIG-I helicases in the recognition of RNA viruses. Nature *441*, 101-105.

Kedersha, N., Chen, S., Gilks, N., Li, W., Miller, I. J., Stahl, J., & Anderson, P. (2002). Evidence that ternary complex (eIF2-GTP-tRNAi Met)–deficient preinitiation complexes are core constituents of mammalian stress granules. Molecular biology of the cell, 13(1), 195-210.

Kedersha, N. L., Gupta, M., Li, W., Miller, I., & Anderson, P. (1999). RNA-binding proteins TIA-1

and TIAR link the phosphorylation of eIF-2α to the assembly of mammalian stress granules. The Journal of cell biology, 147(7), 1431-1442.

Kedersha, N., Panas, M.D., Achorn, C.A., Lyons, S., Tisdale, S., Hickman, T., Thomas, M., Lieberman, J., McInerney, G.M., Ivanov, P.*, et al.* (2016). G3BP–Caprin1–USP10 complexes mediate stress granule condensation and associate with 40S subunits. Journal of Cell Biology, 212(7), e201508028.

Komander D., and Rape M. (2012). The ubiquitin code. Annual Review of Biochemistry 81, 203–229.

Kowalinski, E., Lunardi, T., McCarthy, A.A., Louber, J., Brunel, J., Grigorov, B., Gerlier, D., and Cusack, S. (2011). Structural basis for the activation of innate immune pattern-recognition receptor RIG-I by viral RNA. Cell 147, 423-435.

Kuri, T., Habjan, M., Penski, N., and Weber, F. (2010). Species-independent bioassay for sensitive quantification of antiviral type I interferons. Virol J 7, 50.

Lang, X., Tang, T., Jin, T., Ding, C., Zhou, R., and Jiang, W. (2017). TRIM65-catalized ubiquitination is essential for MDA5-mediated antiviral innate immunity. J Exp Med 214: 459–473.

Langereis, M. A., Feng, Q., and van Kuppeveld, F. J. (2013). MDA5 localizes to stress granules, but this localization is not required for the induction of type I interferon. Journal of virology, 87(11), 6314-6325.

Lassig, C., and Hopfner, K.P. (2017). Discrimination of cytosolic self and non-self RNA by RIG-I-like receptors. J Biol Chem 292, 9000-9009.

Li, M.M., Lau, Z., Cheung, P., Aguilar, E.G., Schneider, W.M., Bozzacco, L., Molina, H., Buehler, E., Takaoka, A., Rice, C.M., *et al.* (2017). TRIM25 Enhances the Antiviral Action of Zinc-Finger Antiviral Protein (ZAP). PLoS Pathog 13, e1006145.

Li, Y., Banerjee, S., Goldstein, S.A., Dong, B., Gaughan, C., Rath, S., Donovan, J., Korennykh, A., Silverman, R.H., and Weiss, S.R. (2017). Ribonuclease L mediates the cell-lethal phenotype of double-stranded RNA editing enzyme ADAR1 deficiency in a human cell line. Elife, 6, e25687.

Lu, C., Xu, H., Ranjith-Kumar, C.T., Brooks, M.T., Hou, T.Y., Hu, F., Herr, A.B., Strong, R.K., Kao, C.C., and Li, P. (2010). The structural basis of 5' Triphosphate Double-Stranded RNA Recognition by RIG-I C-Terminal Domain. Structure *18*, 1032-1043.

Luo, D., Kohlway, A., Vela, A., and Pyle, A.M. (2012). Visualizing the determinants of viral RNA recognition by innate immune sensor RIG-I. Structure 20, 1983-1988.

Manokaran, G., Finol, E., Wang, C., Gunaratne, J., Bahl, J., Ong, E.Z., Tan, H.C., Sessions, O.M., Ward, A.M., Gubler, D.J., *et al.* (2015). Dengue subgenomic RNA binds TRIM25 to inhibit interferon expression for epidemiological fitness. Science 350, 217-221.

McComb, S., Chan, P.K., Guinot, A., Hartmannsdottir, H., Jenni, S., Dobay, M.P., Bourquin, J.P., and Bornhauser, B.C (2019). Efficient apoptosis requires feedback amplification of upstream apoptotic signals by effector caspase-3 or-7. Science Advances, 5(7).

McEwen, E., Kedersha, N., Song, B., Scheuner, D., Gilks, N., Han, A., Chen, J.J., Anderson, P. and Kaufman, R.J. (2005). Heme-regulated inhibitor kinase-mediated phosphorylation of eukaryotic translation initiation factor 2 inhibits translation, induces stress granule

formation, and mediates survival upon arsenite exposure. Journal of Biological Chemistry, 280(17), 16925-16933.

Meyerson, N.R., Zhou, L., Guo, Y.R., Zhao, C., Tao, Y.J., Krug, R.M., and Sawyer, S.L. (2017). Nuclear TRIM25 Specifically Targets Influenza Virus Ribonucleoproteins to Block the Onset of RNA Chain Elongation. Cell Host Microbe 22, 627-638 e627.

Morrone, S.R., Wang, T., Constantoulakis, L.M., Hooy, R.M., Delannoy, M.J., and Sohn, J. (2014). Cooperative assembly of IFI16 filaments on dsDNA provides insights into host defense strategy. Proc Natl Acad Sci U S A 111, E62-71.

Motz, C., Schuhmann, K.M., Kirchhofer, A., Moldt, M., Witte, G., Conzelmann, K.K., and Hopfner, K.-P. (2013). Paramyxovirus V Proteins Disrupt the Fold of the RNA Sensor MDA5 to Inhibit Antiviral Signaling. Science Epub ahead of print.

Myong, S., Cui, S., Cornish, P.V., Kirchhofer, A., Gack, M.U., Jung, J.U., Hopfner, K.-P., and Ha, T. (2009). Cytosolic Viral Sensor RIG-I Is a 5′-Triphosphate–Dependent Translocase on Double-Stranded RNA. Science 323, 1070-1074.

Oh, S.W., Onomoto, K., Wakimoto, M., Onoguchi, K., Ishidate, F., Fujiwara, T., Yoneyama, M., Kato, H., and Fujita, T. (2016). Leader-Containing Uncapped Viral Transcript Activates RIG-I in Antiviral Stress Granules. PLoS Pathog 12, e1005444.

Ohi, M., Li, Y., Cheng, Y., and Walz, T. (2004). Negative staining and image classification - powerful tools in modern electron microscopy. Biol Proced Online 6, 23-34.

Onomoto, K., Jogi, M., Yoo, J.S., Narita, R., Morimoto, S., Takemura, A., Sambhara, S., Kawaguchi, A., Osari, S., Nagata, K., *et al*. (2013). Critical role of an antiviral stress

granule containing RIG-I and PKR in viral detection and innate immunity. PLoS One 7, e43031.

Onomoto, K., Yoneyama, M., Fung, G., Kato, H., & Fujita, T. (2014). Antiviral innate immunity and stress granule responses. Trends in immunology, 35(9), 420-428.

Oshiumi, H., Matsumoto, M., Hatakeyama, S., and Seya, T. (2009). Riplet/RNF135, a RING finger protein, ubiquitinates RIG-I to promote interferon-beta induction during the early phase of viral infection. J Biol Chem 284, 807-817.

Oshiumi, H., Miyashita, M., Inoue, N., Okabe, M., Matsumoto, M., and Seya, T. (2010). The ubiquitin ligase Riplet is essential for RIG-I-dependent innate immune responses to RNA virus infection. Cell Host Microbe 8, 496-509.

Oshiumi, H., Miyashita, M., Matsumoto, M., and Seya, T. (2013). A distinct role of Riplet-mediated K63-Linked polyubiquitination of the RIG-I repressor domain in human antiviral innate immune responses. PLoS Pathog 9, e1003533.

Pakos-Zebrucka, K., Koryga, I., Mnich, K., Ljujic, M., Samali, A., & Gorman, A. M. (2016). The integrated stress response. EMBO reports, 17(10), 1374-1395.

Patel, J.R., Jain, A., Chou, Y.Y., Baum, A., Ha, T., and Garcia-Sastre, A. (2013). ATPase-driven oligomerization of RIG-I on RNA allows optimal activation of type-I interferon. EMBO Rep 14, 780-787.

Peisley, A., Jo, M., Lin, C., Wu, B., Orme-Johnson, M., Walz, T., Hohng, S., and Hur, S. (2012). Kinetic Mechanism for Viral dsRNA Length Discrimination by MDA5 Filament. Proc Natl Acad Sci U S A 109, E3340-3349.

Peisley, A., Lin, C., Bin, W., Orme-Johnson, M., Liu, M., Walz, T., and Hur, S. (2011). Cooperative Assembly and Dynamic Disassembly of MDA5 Filaments for Viral dsRNA Recognition. Proc Natl Acad Sci U S A 108, 21010-21015.

Peisley, A., Wu, B., Xu, H., Chen, Z.J., and Hur, S. (2014). Structural basis for ubiquitin-mediated antiviral signal activation by RIG-I. Nature 509, 110-114.

Peisley, A., Wu, B., Yao, H., Walz, T., and Hur, S. (2013). RIG-I Forms Signaling-Competent Filaments in an ATP-Dependent, Ubiquitin-Independent Manner. Mol Cell 51, 573-583.

Pichlmair, A., Schultz, D.E., Tan, C.P., Naslund, T.I., Liljestrom, P., Weber, F., and Reis e Sousa, C. (2006). RIG-I–Mediated Antiviral Responses to Single-Stranded RNA Bearing 5'-Phosphates. Science *314*, 997-1001.

Rawling, D.C., Fitzgerald, M.E., and Pyle, A.M. (2015). Establishing the role of ATP for the function of the RIG-I innate immune sensor. Elife 4.

Rawling, D.C., and Pyle, A.M. (2014). Parts, assembly and operation of the RIG-I family of motors. Curr Opin Struct Biol 25, 25-33.

Reineke, L. C., Cheema, S. A., Dubrulle, J., and Neilson, J. R. (2018). Chronic starvation induces noncanonical pro-death stress granules. J Cell Sci, 131(19), jcs220244.

Reineke, L. C., and Neilson, J. R. (2019). Differences between acute and chronic stress granules, and how these differences may impact function in human disease. Biochemical pharmacology, 162, 123-131.

Ren, X., Linehan, M.M., Iwasaki, A., and Pyle, A.M. (2019). RIG-I Selectively Discriminates against 5'-Monophosphate RNA. Cell Rep 26, 2019-2027 e2014.

Reuther, P., Gopfert, K., Dudek, A.H., Heiner, M., Herold, S., and Schwemmle, M. (2015). Generation of a variety of stable Influenza A reporter viruses by genetic engineering of the NS gene segment. Sci Rep 5, 11346.

Rodriguez, K.R., and Horvath, C.M. (2013). Amino acid requirements for MDA5 and LGP2 recognition by paramyxovirus V proteins: a single arginine distinguishes MDA5 from RIG-I. J Virol 87, 2974-2978.

Sanchez, J.G., Chiang, J.J., Sparrer, K.M.J., Alam, S.L., Chi, M., Roganowicz, M.D., Sankaran, B., Gack, M.U., and Pornillos, O. (2016). Mechanism of TRIM25 Catalytic Activation in the Antiviral RIG-I Pathway. Cell Rep 16, 1315-1325.

Sanchez, J.G., Okreglicka, K., Chandrasekaran, V., Welker, J.M., Sundquist, W.I., and Pornillos, O. (2014). The tripartite motif coiled-coil is an elongated antiparallel hairpin dimer. Proc Natl Acad Sci U S A 111, 2494-2499.

Schlee, M., Roth, A., Hornung, V., Hagmann, C.A., Wimmenauer, V., Barchet, W., Coch, C., Janke, M., Mihailovic, A., Wardle, G., *et al.* (2009). Recognition of 5'triphosphate by RIG-I helicase requires short blunt double-stranded RNA as contained in panhandle of negative-strand virus. Immunity 31, 25-34.

Shi, Y., Yuan, B., Zhu, W., Zhang, R., Li, L., Hao, X., Chen, S., and Hou, F. (2017). Ube2D3 and Ube2N are essential for RIG-I-mediated MAVS aggregation in antiviral innate immunity. Nat Commun 8, 15138.

Silva, J.M., Rodrigues, S., Sampaio-Marques, B., Gomes, P., Neves-Carvalho, A., Dioli, C., Soares-

Cunha, C., Mazuik, B.F., Takashima, A., Ludovico, P., *et al*. (2019). Dysregulation of autophagy and stress granule-related proteins in stress-driven Tau pathology. Cell Death & Differentiation, 26(8), 1411-1427.

Sohn, J., and Hur, S. (2016). Filament assemblies in foreign nucleic acid sensors. Curr Opin Struct Biol 37, 134-144.

Srivastava, S. P., Kumar, K. U., and Kaufman, R. J. (1998). Phosphorylation of eukaryotic translation initiation factor 2 mediates apoptosis in response to activation of the double-stranded RNA-dependent protein kinase. Journal of Biological Chemistry, 273(4), 2416-2423.

Strahle, L., Garcin, D., and Kolakofsky, D. (2006). Sendai virus defective-interfering genomes and the activation of interferon-beta. Virology *351*, 101-111.

Uzri, D., and Gehrke, L. (2009). Nucleotide sequences and modifications that determine RIG-I/RNA binding and signaling activities. J Virol *83*, 4174-4184.

Wang, Y., Ludwig, J., Schuberth, C., Goldeck, M., Schlee, M., Li, H., Juranek, S., Sheng, G., Micura, R., Tuschl, T.*, et al.* (2010). Structural and functional insights into 5'-ppp RNA pattern recognition by the innate immune receptor RIG-I. Nat Struct Mol Biol *17*, 781-787.

Weinert, C., Morger, D., Djekic, A., Grutter, M.G., and Mittl, P.R. (2015). Crystal structure of TRIM20 C-terminal coiled-coil/B30.2 fragment: implications for the recognition of higher order oligomers. Sci Rep 5, 10819.

Wek, R. C. (2018). Role of eIF2α kinases in translational control and adaptation to cellular stress. Cold Spring Harbor perspectives in biology, 10(7), a032870.

Wu, B., Huoh, Y.S., and Hur, S. (2016). Measuring Monomer-to-Filament Transition of MAVS as an In Vitro Activity Assay for RIG-I-Like Receptors. Methods Mol Biol 1390, 131-142.

Wu, B., and Hur, S. (2015). How RIG-I like receptors activate MAVS. Curr Opin Virol 12, 91-98.

Wu, B., Peisley, A., Richards, C., Yao, H., Zeng, X., Lin, C., Chu, F., Walz, T., and Hur, S. (2013). Structural Basis for dsRNA Recognition, Filament Formation, and Antiviral Signal Activation by MDA5. Cell 152, 276-289.

Wu, B., Peisley, A., Tetrault, D., Li, Z., Egelman, E.H., Magor, K.E., Walz, T., Penczek, P.A., and Hur, S. (2014). Molecular imprinting as a signal activation mechanism of the viral RNA sensor RIG-I. Mol Cell 55, 511-523.

Wu, X., and Karin, M. (2015). Emerging roles of Lys63-linked polyubiquitylation in immune responses. Immunol Rev 266, 161-174.

Yoneyama, M., Kikuchi, M., Natsukawa, T., Shinobu, N., Imaizumi, T., Miyagishi, M., Taira, K., Akira, S., and Fujita, T. (2004). The RNA helicase RIG-I has an essential function in double-stranded RNA-induced innate antiviral responses. Nat Immunol 5, 730-737.

Yoneyama, M., and Fujita, T. (2010). Recognition of viral nucleic acids in innate immunity. Rev Med Virol 20, 4-22.

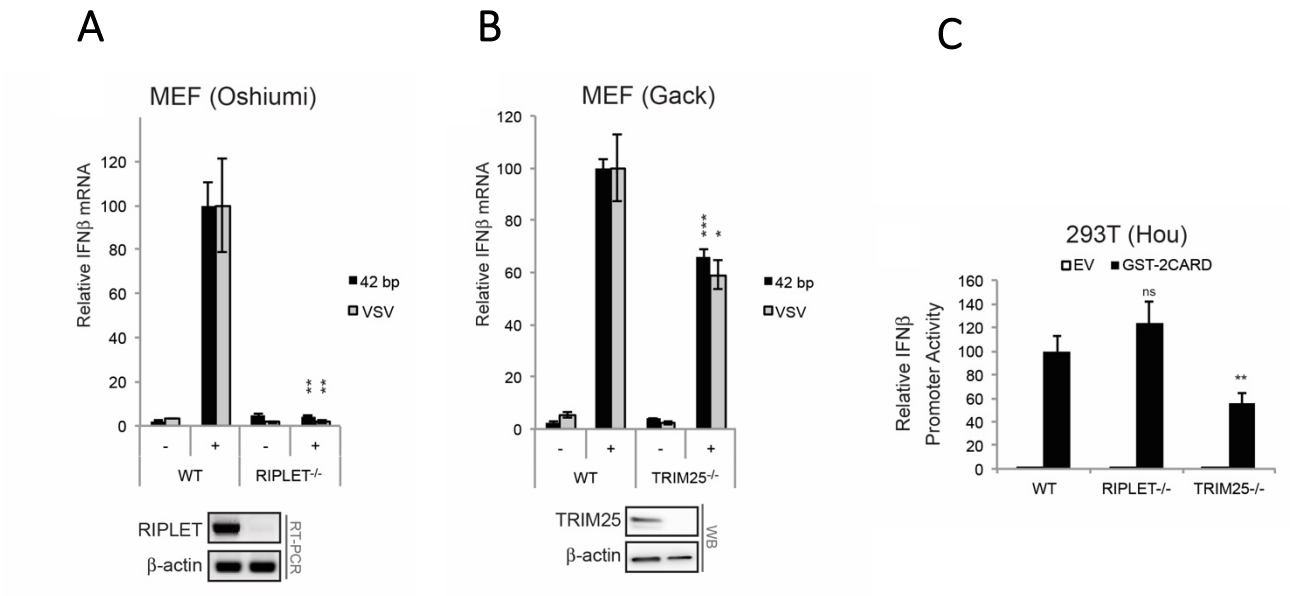
Zeng, W., Sun, L., Jiang, X., Hou, F., Adhikari, A., Xu, M., and Chen, Z.J. (2010). Reconstitution of the RIG-I pathway reveals a signaling role of unanchored polyubiquitin chains in innate immunity. Cell 141.

Zhang, P., Fan, B., Yang, P., Temirov, J., Messing, J., Kim, H. J., & Taylor, J. P. (2019). Chronic optogenetic induction of stress granules is cytotoxic and reveals the evolution of ALS-FTD pathology. Elife, 8, e39578.

Zheng, X., Wang, X., Tu, F., Wang, Q., Fan, Z., and Gao, G. (2017). TRIM25 Is Required for the Antiviral Activity of Zinc Finger Antiviral Protein. J Virol 91.

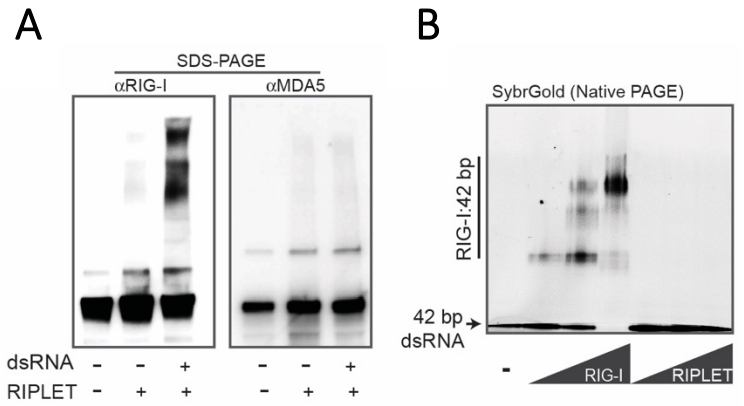
Zhou, W., Whiteley, A.T., de Oliveira Mann, C.C., Morehouse, B.R., Nowak, R.P., Fischer, E.S., Gray, N.S., Mekalanos, J.J., and Kranzusch, P.J. (2018). Structure of the Human cGAS-DNA Complex Reveals Enhanced Control of Immune Surveillance. Cell 174, 300-311 e311.

Appendix 2: supplemental Figures



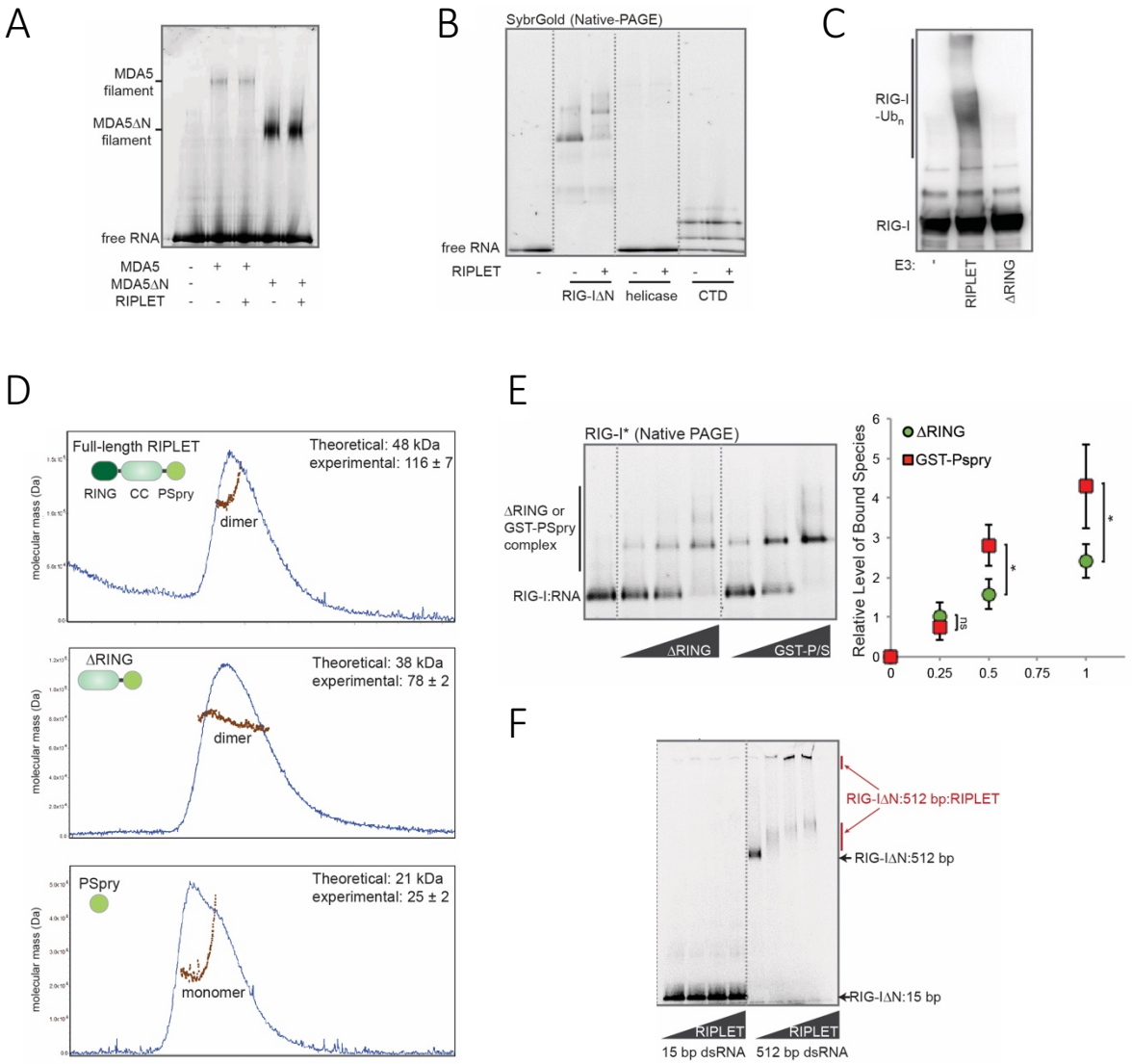
Supplemental Figure 1 Related to Figure 2.1

S1A-B) MEF (WT and RIPLET-/-) and MEF (WT and TRIM25-/-) were obtained from Oshiumi (Oshiumi et al., 2010) and Gack (Gack et al., 2007) laboratories, respectively. Cells were stimulated with 42 bp dsRNA with 5'ppp (0.2 μg) or VSV (MOI=1), and the antiviral signaling activity was measured by the IFN-β mRNA level (using GAPDH as an internal control) and normalized against the WT values. **S1C)** Relative signaling activity of RIG-I 2CARD fused to GST (GST-2CARD) (50 ng) in 293T cells (WT, RIPLET-/- or TRIM25-/-, from the Hou lab (Shi et al., 2017)), as measured by the IFN-β promoter reporter assay. Note that antiviral signaling by GST-2CARD occurs in a RIPLET-independent manner because, as shown in Figure 3A, RIPLET does not recognize isolated 2CARD.



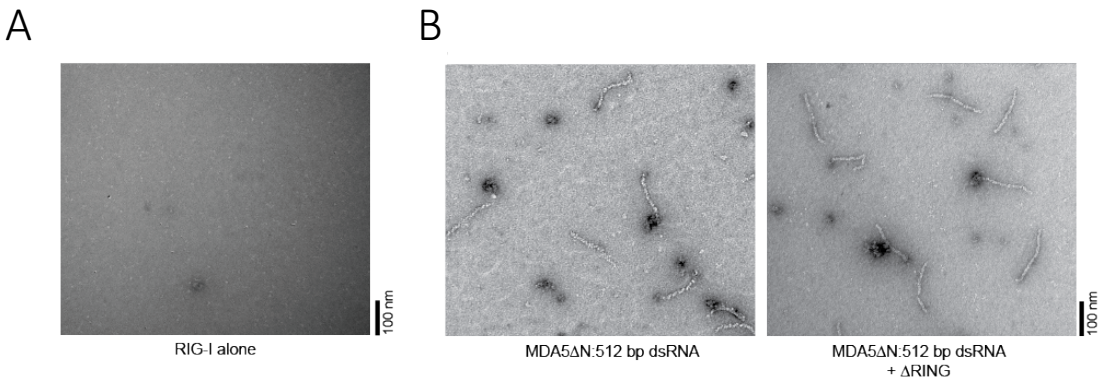
Supplemental Figure 2 Related to Figure 2.2

S2A) *In vitro* ubiquitination of RIG-I and MDA5 by RIPLET. RIG-I or MDA5 (0.5 μM) was incubated with RIPLET (0.25 μM) in the presence or absence of their preferred dsRNA substrates (42 bp for RIG-I and 512 bp for MDA5, 1 ng/μl). Reactions were performed as in Figure 2A, and analyzed by anti-RIG-I or anti-MDA5 blot. **S2B)** RNA binding activity of RIG-I and RIPLET, as measured by native gel shift assay. An increasing concentration of RIG-I or RIPLET (0.25, 0.5, 1 μM) was incubated with 42 bp dsRNA and analyzed by native PAGE. Gel image was obtained using fluorescence of RNA stained with SybrGold.


A
MDA5 filament
MDA5ΔN filament
free RNA
MDA5 - + +
MDA5ΔN - + +
RIPLET - - + - +
B
SybrGold (Native-PAGE)
free RNA
RIPLET - - + - + - +
RIG-IΔN helicase CTD
C
RIG-I -Ub$_n$
RIG-I
E3: ' RIPLET ΔRING
D
Full-length RIPLET
RING CC PSpry
Theoretical: 48 kDa
experimental: 116 ± 7
dimer
molecular mass (Da)
ΔRING
Theoretical: 38 kDa
experimental: 78 ± 2
dimer
PSpry
Theoretical: 21 kDa
experimental: 25 ± 2
monomer
E
RIG-I* (Native PAGE)
ΔRING or GST-PSpry complex
RIG-I:RNA
ΔRING
GST-P/S
ΔRING
GST-Pspry
Relative Level of Bound Species
ns
*
*
F
RIG-IΔN:512 bp:RIPLET
RIG-IΔN:512 bp
RIG-IΔN:15 bp
RIPLET
RIPLET
15 bp dsRNA
512 bp dsRNA

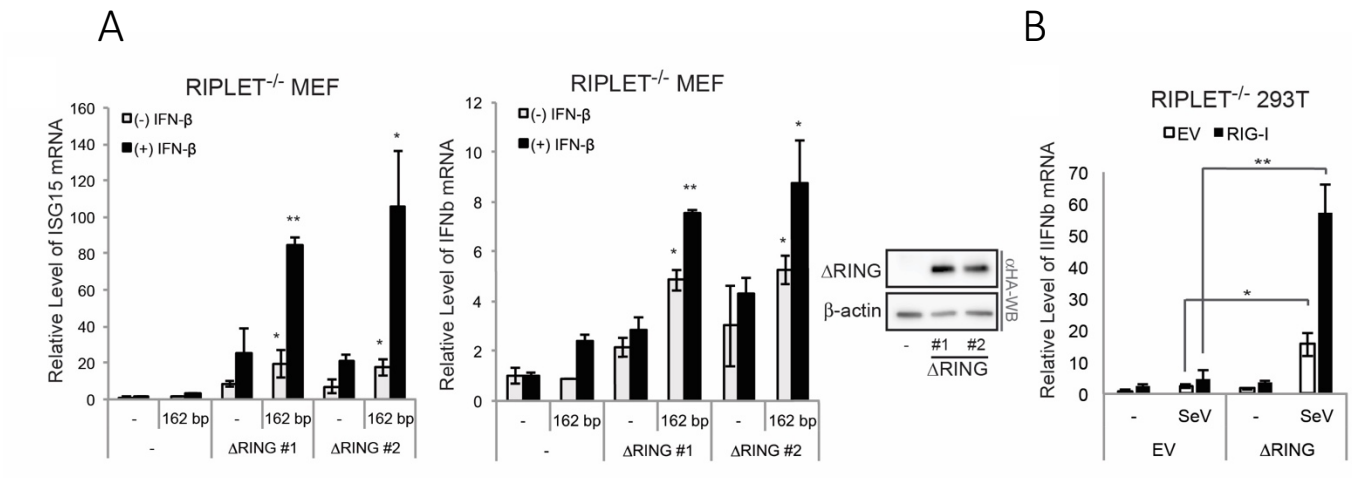
Supplementary Figure 3 Related to Figure 2.3

S3A) Native gel shift assay of MDA5 with RIPLET. 512 bp dsRNA was visualized using fluorescence of the SybrGold stain. **S3B)** Native gel shift assay of RIG-I variants with RIPLET. 42 bp dsRNA (1 ng/μl) was incubated with RIG-IΔN, the helicase domain or CTD (0.5 μM), in the presence or absence of RIPLET (0.5 μM). 42 bp dsRNA was visualized using fluorescence of the SybrGold stain. **S3C)** *In vitro* Ub chain synthesis by RIPLET and ΔRING. **S3D)** Multi-angle light scattering (MALS) traces of full-length RIPLET, ΔRING and PSpry. Theoretical and experimental molecular weights are shown on the upper right corner. Only PSpry exists as a monomer, while full-length RIPLET and ΔRING are constitutive dimers. Blue and brown traces indicate OD280 and estimated molecular weight, respectively. **S3E)** Native gel shift assay to compare the RIG-I binding efficiency of ΔRING and GST-PSpry. Right: the bound species was quantified using densitometry (mean ± s.d., n = 3). * $p < 0.05$, ** $p < 0.01$, ***$p < 0.001$, ns, not significant (unpaired t test). **S3F)** Native gel shift assay to monitor the interaction between RIG-I and RIPLET. Fluorescently labeled RIG-IΔN (300 nM) was incubated with RIPLET (0, 150, 300, 600 nM) in the presence or absence of 15 bp or 512 bp dsRNA (2.5 ng/μl), and the complex was analyzed by native gel using RIG-I fluorescence. Note that there are two populations of the RIG-I:512 bp:RIPLET complex, one migrating into the gel and the other remaining in the gel well. All data are representative of three independent experiments.



Supplementary Figure 4 related to figure 2.4

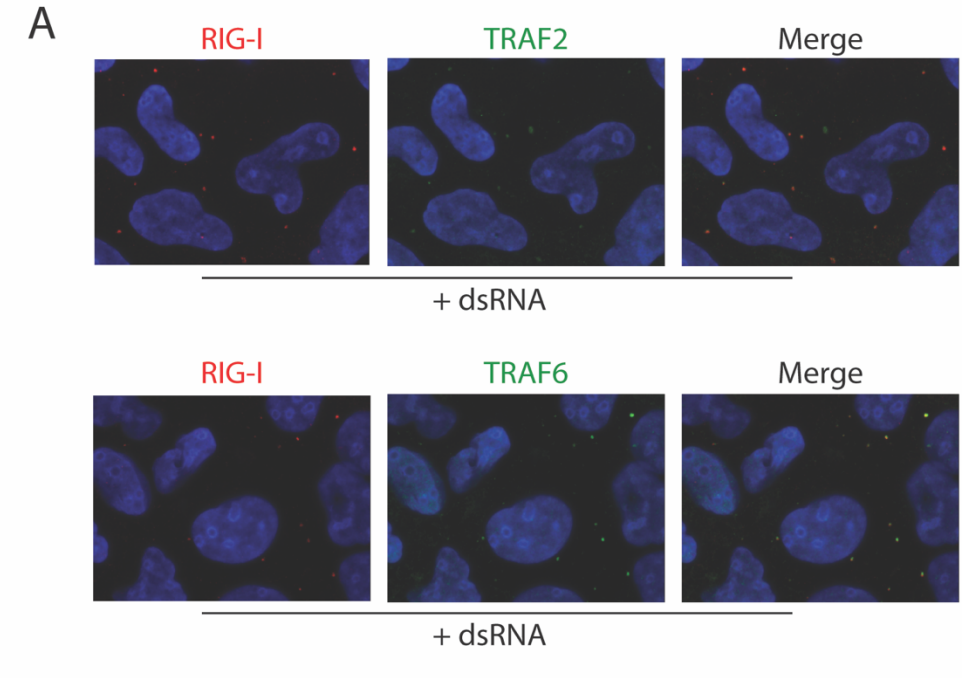
S4A) Representative EM image of RIG-I protein alone (0.5 μM). **S4B)** Representative EM images of MDA5ΔN filaments (0.4 μM) formed on 512 bp dsRNA (1 ng/μl), in the presence and absence of ΔRING (0.4 μM). Due to the instability of the MDA5 filament on EM grids, ADP•AlF4 (1 mM) was added prior to the grid preparation. Previous EM analysis of MDA5 filaments similarly required ADP•AlF4 to stabilize the filament on the grid (Peisley et al., 2011; Wu et al., 2013).



Supplementary Figure 5 related to figure 2.6

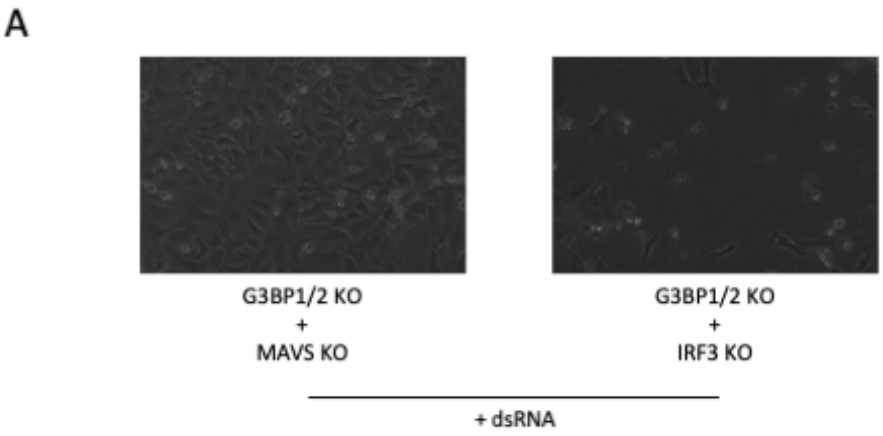
S5A) Relative level of antiviral signaling in RIPLET-/- MEFs stably expressing ΔRING upon stimulation with 162 bp dsRNA (0.2 μg). Two different clones of RIPLET-/- MEF reconstituted with HA-tagged ΔRING were used (see WB on the right). In a subset of samples, IFN-β (10 ng/ml) was added to the medium (24 hrs prior to RNA transfection) to increase the level of RIG-I. The RIG-I-stimulatory activity of ΔRING was evident even with the basal level of RIG-I and stably expressing ΔRING, but IFN-β further enhanced the effect of ΔRING. This is consistent with the notion that the higher level of RIG-I allows more efficient filament formation on dsRNA and thus, more efficient filament bridging by ΔRING. See also (B).

S5B) Relative level of antiviral signaling in RIPLET-/- 293T upon stimulation with 162 bp dsRNA (0.2 μg), with and without complementation with ΔRING. ΔRING was transiently expressed (20 ng) together with RIG-I (10 ng) or by itself in RIPLET-/- 293T. The RIG-I-stimulatory activity of ΔRING was evident even with endogenous RIG-I, but ectopic expression of RIG-I further enhanced the effect of ΔRING.



Supplementary Figure 6 related to figure 3.1

S6A) Representative immunofluoresce images of endogenous RIG-I and endogenous TRAF2 (top) and endogenous TRAF6 (bottom) in the presence of 162bp dsRNA (0.5µg). Cells were fixed 6 hours post-stimulation.



Supplementary Figure 7 related to figure 3.3

S7A) Representative microscopy images of G3BP1/2 MAVS KO and G3BP1/2 IRF3 KO U2OS in the presence of 162bp dsRNA (1µg). Images were taken 24 hours post-stimulation.